UNIVERSIDADE ESTADUAL DE CAMPINAS

INSTITUTO DE QUÍMICA

SAMILE BEZERRA DE AGUIAR

DEVELOPMENT OF LAPONITE-BASED NANOSTRUCTURED MATERIALS FOR APPLICATIONS IN CATALYSIS AND DRUG DELIVERY

DESENVOLVIMENTO DE MATERIAIS NANOESTRUTURADOS À BASE DE LAPONITA PARA APLICAÇÕES EM CATÁLISE E VECTORIZAÇÃO DE FÁRMACOS

CAMPINAS
2022

SAMILE BEZERRA DE AGUIAR

DEVELOPMENT OF LAPONITE-BASED NANOSTRUCTURED MATERIALS FOR APPLICATIONS IN CATALYSIS AND DRUG DELIVERY

DESENVOLVIMENTO DE MATERIAIS NANOESTRUTURADOS À BASE DE LAPONITA PARA APLICAÇÕES EM CATÁLISE E VECTORIZAÇÃO DE FÁRMACOS

Dissertação de Mestrado apresentada ao Instituto de Química da Universidade Estadual de Campinas como parte dos requisitos exigidos para a obtenção do título de Mestra em Química na área de Química Orgânica.

Master's Dissertation presented to the Institute of Chemistry of the University of Campinas as part of the requirements to obtain the title of Master in Chemistry in the area of Organic Chemistry.

Supervisor: Profa. Dra. Cátia Cristina Capelo Ornelas Megiatto

ESTE EXEMPLAR CORRESPONDE À VERSÃO FINAL DA DISSERTAÇÃO DE MESTRADO DEFENDIDA PELA ALUNA SAMILE BEZERRA DE AGUIAR, E ORIENTADA PELA PROFA. DRA. CÁTIA CRISTINA CAPELO ORNELAS MEGIATTO

CAMPINAS
2022

Ficha catalográfica
Universidade Estadual de Campinas
Biblioteca do Instituto de Química
Simone Luiz Alves - CRB 8/9094

Ag93d

Aguiar, Samile Bezerra de, 1997-
Development of laponite-based nanostructured materials for applications in catalysis and drug delivery / Samile Bezerra de Aguiar. – Campinas, SP : [s.n.], 2022.

Orientador: Cátia Cristina Capelo Ornelas Megiatto.
Dissertação (mestrado) – Universidade Estadual de Campinas, Instituto de Química.

1. Hidrogéis. 2. Nanohidrogel. 3. Catálise. 4. Sistemas de liberação de medicamentos. I. Ornelas, Cátia, 1980-. II. Universidade Estadual de Campinas. Instituto de Química. III. Título.

Informações para Biblioteca Digital

Título em outro idioma: Desenvolvimento de materiais nanoestruturados à base de laponita para aplicações em catálise e vectorização de fármacos
Palavras-chave em inglês:
Hydrogels
Nanohydrogel
Catalysis
Drug delivery systems
Área de concentração: Química Orgânica
Titulação: Mestra em Química na área de Química Orgânica
Banca examinadora:
Cátia Cristina Capelo Ornelas Megiatto
Pablyana Leila Rodrigues da Cunha
Edvaldo Sabadini
Data de defesa: 25-02-2022
Programa de Pós-Graduação: Química

Identificação e informações acadêmicas do(a) aluno(a)
- ORCID do autor: https://orcid.org/0000-0002-9543-0462
- Currículo Lattes do autor: http://lattes.cnpq.br/2529588190691894

EVALUATION COMMITTEE

BANCA EXAMINADORA

Profa. Dra. Cátia Cristina Capelo Ornelas Megiatto (Orientadora)

Profa. Dra. Pablyana Leila Rodrigues da Cunha (Universidade Federal do Ceará, UFC)

Prof. Dr. Edvaldo Sabadini (IQ – Universidade Estadual de Campinas, UNICAMP)

A Ata da defesa com as respectivas assinaturas dos membros encontra-se no processo de vida acadêmica do aluno.

Este exemplar corresponde à redação final da Dissertação de Mestrado defendida pela aluna **SAMILE BEZERRA DE AGUIAR**, aprovada pela Comissão Julgadora em 25 de fevereiro de 2022.

Dedico esta dissertação ao que é mais importante na minha vida: a Deus, aos meus pais e meus herois, Maria e José; ao meu irmão e meu exemplo de ser humano, Windson; e ao meu incrível e paciente companheiro de vida, Joan. A vocês, agradeço por sempre apoiarem os meus sonhos e por compreenderem a distância durante esta etapa da vida. Sem vocês eu nunca teria chegado até aqui!

AGRADECIMENTOS

À professora *Cátia Ornelas*, por ter me aceito em seu grupo de pesquisa e por gentilmente ter me orientado ao longo desse Mestrado tão turbulento. Agradeço por ter tirado minhas dúvidas durante todo esse período, mesmo sendo algumas tão triviais, e por não ter desistido de mim mesmo com tantas dificuldades em uma pandemia.

À pós-doct do grupo de pesquisa, *Carolyne B. Braga*, por ter me ajudado desde o início com os trabalhos de bancada e ter me ensinado diversos procedimentos com tanta dedicação e paciência! Agradeço pelas trocas de conhecimento e pelos vários momentos de conversas, pelas orientações pessoais e pelo apoio dado nos vários momentos que passei por dificuldades pessoais.

Aos meus amigos e moradores da "Vila": *Guida Hellen* (obrigada por ter chegado em um momento tão importante e por ter se tornado uma amiga tão essencial), *Herllan Vieira* (um agradecimento especial pelas risadas e por tantos ensinamentos), *João Pedro* (obrigada pelos momentos de reflexão e pelas risadas geradas ao tentar cozinhar) e *Nilvan Alves* (obrigada por suportar os meus vários barulhos em pleno início de manhã, às 5h). A vocês que chegaram como amigos/conhecidos e hoje se tornaram minha segunda família, muito obrigada por terem ajudado nesse período acadêmico e, principalmente, agradeço por terem me dado suporte pessoal e emocional durante todo o caos desse período.

Aos meus amigos que indiretamente me ajudaram a chegar até aqui (Rodrigo Costa, Luís Felipe, Brener Arruda, Ludmilla e outros).

Aos membros titulares da banca, Prof. Dr. Edvaldo Sabadini e Profa. Dra. Pablyana Rodrigues, por terem aceitado gentil e prontamente o convite de participação na banca. Agradeço pelas contribuições feitas desde já.

Ao Conselho Nacional de Desenvolvimento Científico e Tecnológico (CNPq), pela bolsa concedida durante esse Mestrado (Processo n° 132403/2020-0), que contribuiu diretamente para a possibilidade de realização deste trabalho.

À UNICAMP, e em especial ao Instituto de Química (IQ) pela excelente infraestrutura disponibilizada.

The authors would like to thank LNNano/CNPEM for the access to the electron microscopy facility and technical support, in the execution of the proposal FT20220278.

This study was financed in part by the Coordenação de Aperfeiçoamento de Pessoal de Nível Superior - Brasil (CAPES) - Finance Code 001.

RESUMO

Nanopartículas metálicas tais como nanopartículas de ouro, prata e platina desempenham um papel importante como catalizadores heterogêneos. A fim de aumentar a estabilidade e evitar a formação de aglomerados metálicos, estes tipos de nanopartículas podem ser ancoradas em materiais de suporte. Hidrogéis à base de Laponita e poliacrilato de sódio podem agir como um ótimo material de suporte para a síntese *in situ* de nanopartículas metálicas, pois o processo de gelificação ocorre rapidamente através de interações não covalentes entre os nanodiscos de Laponita, o poliacrilato e os cátions adicionados. Neste trabalho, a eventual formação *in situ* de nanopartículas de Au, Ag e Pt dentro do hidrogel foi avaliada por espectroscopia de UV-Vis e TEM. Os materiais também foram caracterizados por espectroscopia de infravermelho (FTIR), e as propriedades mecânicas dos hidrogéis formados foram analisadas por reologia, que mostrou uma propriedade de gel para todos os hidrogéis, com um módulo de armazenamento (G') maior que o módulo de perda (G"), e o hidrogel com Pt possuindo o maior valor G' (23 kPa). A aplicação de AuNPs, AgNPs e PtNPs suportadas nos hidrogéis foi testada como catalisador na reação de redução do conhecido poluente 4-nitrofenol (4-NP). O melhor hidrogel com AuNPs mostrou a maior atividade catalítica com rendimento de 99% de redução, enquanto os melhores hidrogéis com AgNPs e PtNPs resultaram em rendimentos de 97% e 84%, respectivamente.

Uma versão nanométrica do hidrogel à base de Laponita foi testada como um nanocarreador de coquetel de fármacos anticâncer. Os nanohidrogéis biodegradáveis foram sintetizados pela técnica de miniemulsão inversa com fármacos anticâncer (Cisplatina, CP; 5-Fluorouracila, 5-FU; e Ciclofosfamida, CPA) co-encapsulados. Os nanohidrogéis foram obtidos com um tamanho médio entre 60-190 nm, que é um tamanho apropriado para ser aplicado como nanocarreador de fármacos contra células cancerígenas. Nanomateriais com diferentes razões molares de 5-FU, CP e CPA foram aplicados em células MCF-7 e HeLa (células de câncer de mama e adenocarcinoma cérvix, respectivamente) por 48h (a 37 °C), e todos os materiais com 5-FU e CP apresentaram um IC_{50} menor que os fármacos em solução. O índice de combinação (CI) para cada formulação 5-FU+CP foi calculado de acordo com o método de Chou-Talalay (CI<1, =1 ou >1 para, respectivamente, efeito sinérgico, aditivo ou antagônico). Duas de três combinações com maior proporção de 5-FU resultaram em sinergismo contra as células MCF-7 (câncer de mama).

Os resultados obtidos com esse trabalho demostram a versatilidade de materiais nanoestruturados à base de Laponita para aplicação tanto em catálise quanto em entrega de fármacos.

ABSTRACT

Metal nanoparticles such as gold, silver and platinum nanoparticles play a notable role as heterogenous catalysts. To increase stability and prevent the formation of large metal aggregates, these types of nanoparticles can be anchored onto supporting materials. Hydrogels based on Laponite and sodium polyacrylate can act as a great support material for *in situ* synthesis of metallic nanoparticles, because the gelification process occurs rapidly through ionic interactions between the Laponite nanodiscs, the polymer (polyacrylate) and the cations added. In this work, the eventual *in situ* formation of Au, Ag and Pt nanoparticles inside the hydrogels was evaluated by UV-Vis spectroscopy and TEM. The resulting hydrogels were also characterized by FTIR spectroscopy, and their mechanical properties were analyzed by rheology that showed that all hydrogels have a gel-like behavior, with G' higher than G''. The hydrogel with Pt presented the higher G' value (23 kPa) for all studied Laponite-based hydrogels. The application of the AuNPs, AgNPs and PtNPs supported in the hydrogels as catalyst was tested for the reduction of known poluent 4-nitrophenol (4-NP). The best hydrogel with AuNPs showed the higher catalyst activity with 99% yield of reduction, while the best hydrogels with AgNPs and PtNPs resulted in 97% and 84% yield, respectively.

A nanosized version of the Laponite-based hydrogel was tested as a nanocarrier for cancer drug cocktails. Biodegradable nanohydrogels were formulated by inverse miniemulsion technique with the anticancer drugs cisplatin (CP), 5-fluorouracil (5-FU) and cyclophosphamide (CPA) co-encapsulated. The nanohydrogels were obtained with an average size between 60 – 190 nm, which is an appropriate size to be applied as a nanocarrier of drugs against cancer cells. Nanomaterials with different molar ratios of 5-FU, CP and CPA were applied in MCF-7 and HeLa cells (human breast cancer and human cervix adenocarcinoma cells, respectively) for 48h (at 37 °C), and all materials with 5-FU and CP presented an IC_{50} lower than the free drugs. The combination index (CI) for each combo 5-FU+CP was calculated according to the Chou-Talalay method (CI<1, =1 or >1 to, respectively, synergistic, additive, or antagonistic effect). Two out of three combinations with higher ratio of 5-FU resulted in synergism against MCF-7 cells.

The results obtained with these two works demonstrate the versatility of Laponite-based nanostructured materials for application in both catalysis and drug delivery.

SUMMARY

1. INTRODUCTION

1.1 Laponite-based hydrogels

Hydrogels are water-based three-dimensional crosslinked networks consisting of polymer chains that can be natural, synthetic or even the combination thereof, and, as the name suggests, can absorb and retain large amounts of water without disintegrating.[1] The hydrogel's network structure can be formed by chemical crosslinking through covalent bonds, or physical crosslinking (non-covalent interactions),[2] in which physical hydrogels are formed.[3]

Physical hydrogels composed of clay and polymers have been gaining attention due to possibility of application in several research areas. The inclusion of clay into polymeric hydrogels can result in improvement of mechanical properties.[3] Smectite clay minerals, like the synthetic Laponite, are often used due to their layered structure that, when dispersed in water, exfoliates releasing the exchangeable interlayer cations (Na^+ in Laponite), increasing the viscosity of solution, and eventually forming physically crosslinked hydrogels.[2]

Laponite (Lap) is a synthetic silicate with nanodisc shape and empirical formula $Na^+_{0.7}[(Si_8Mg_{5.5}Li_{0.3})O_{20}(OH)_4]^-_{0.7}$. The layered structure of this silicate consists of one octahedral (O) sheet of Mg-O between two tetrahedral (T) sheets of Si-O (*i.e.*,TOT-type) (Figure 1).[4] Each Laponite nanodisc have 25 nm in diameter with less than 1 nm of thickness, with the faces having negative charge and the edges present pH-dependent positive charges, presenting an overall net negative charge.[4]

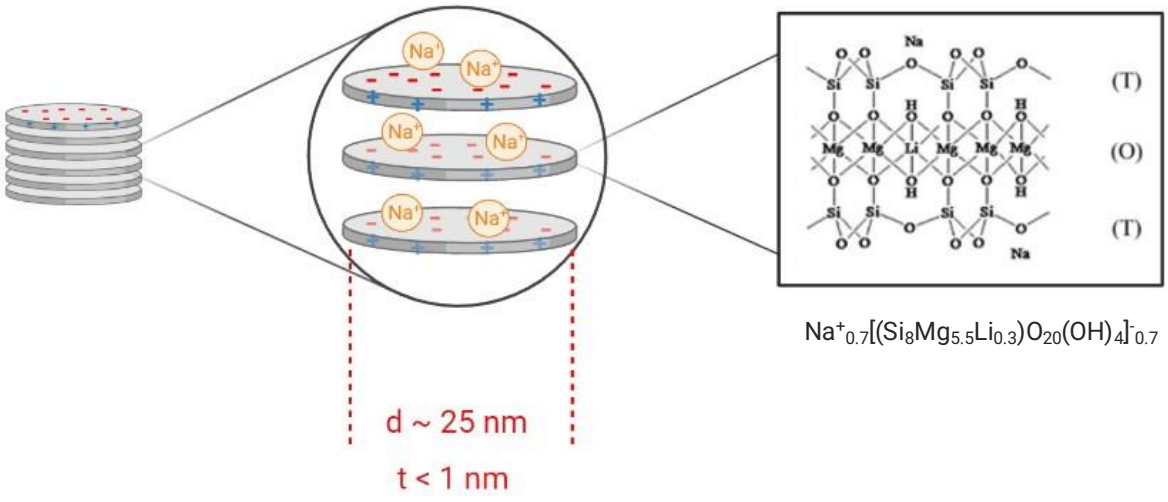

Figure 1. Schematic representation of Laponite nanodiscs and its chemical structure in the solid state (d = diameter; t = thickness).

In water, the Lap-Lap interactions involve a series of electrostatic attractions (between the faces and the edges), repulsion (face with face or edge with edge) and van der Waals attractions. Although, some reports state that the high viscosity of Laponite solutions are gels formed by the fractal network from the face-edge attraction forces ("house of cards" structure demonstrated in figure 2),[5] the real cause of viscosity is still controversial. Some studies suggest[4] that the Lap suspensions with lower wt % at low ionic strength form colloidal Wigner glasses due to the mainly electrostatic repulsion that keeps the nanodiscs apart from each other.[6,7]

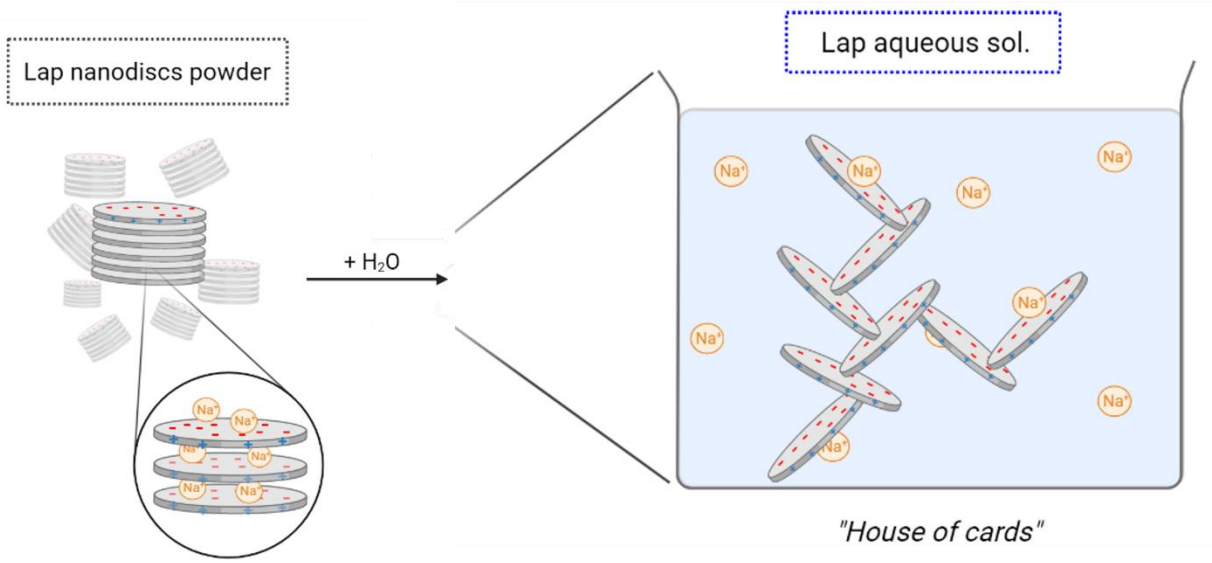

Figure 2. Schematic representation of Laponite nanodiscs interactions ("House of cards") when dispersed in water.

Our research group have recently developed a nonswellable hydrogel material based on non-covalent interaction between Laponite nanodiscs, polyacrylate and a variety of salts.[8] These materials have been showing interesting mechanical properties and our group is currently exploring their potential applications in nanomedicine and in catalysis.

1.1.1 Laponite-based hydrogels for in-situ formation of catalytic active metal nanoparticles

Among the various applications of hydrogels, including biomaterials for nanomedicine and tissue engineering, and materials for environmental remediation, hydrogels have been reported as support materials for metallic nanoparticles due to their interesting network.[9,10] Metallic nanoparticles, such as Ag, Au, Pd and Pt NPs, have been used for different applications

such as sensors, electronic devices, and material science, but thanks to their unique physical and chemical properties such as high surface-area-to-volume ratio, these nanoparticles have become interesting materials for heterogeneous catalysis.[11–13] To ensure high catalytic activity, it is important to control the particle's size, dispersity and shape, which can cause differences in their electronic structure and in the surface atomic arrangement affecting directly their catalytic activity.[14]

1.2 Materials in Nanotechnology

The concept of Nanotechnology was introduced by Richard Feynman in the 50's in its famous conference "There is plenty of room in the bottom". Since then, a lot of research has been dedicated to develop new nanomaterials and new characterization techniques for such small entities. Nanoparticles can be defined as a particulate material with at least one dimension in the range of 1 – 100 nm, although it is usually accepted if the material is smaller than 500 nm. Nanoparticles have several properties that are not found in their bulk material, like high surface-to-volume ratio and unique optical, magnetic, thermal, and reactivity properties.[15] There are several types of nanomaterials that include dendrimers, micelles, vesosomes, metal nanoparticles, polymeric nanoparticles, nanohydrogels, rotaxanes, catenanes, carbon nanotubes, graphene nanosheets, clay nanodiscs, among others.

In the broad field of nanomaterials, nanohydrogels are interesting materials that combine properties and characteristics of both hydrogels and nanoparticles.[16] Nanohydrogels can be defined as nanostructured hydrogels that are composed of crosslinked polymeric networks and have a size range of 1-200 nm.[17] Nanohydrogels, like other nanoparticles, are suitable for a wide range of applications including food science and food industry,[18] and medicine.[19,20]

Nanoparticles have some interesting advantages as nanocarriers for the treatment of diseases, when compared to conventional molecular agents, such as protection of encapsulated drugs against early degradation, and the benefit that the nanoplatform can be designed for a controlled and sustained release of drugs at the target site.[21] A variety of nanohydrogels have been studied as drug delivery systems, with the advantage of their unique structure and properties that include high biocompatibility due to the large water content, their hydrophilic interior capable of load and protect hydrophilic drugs and their high stability for prolonged

circulation in the bloodstream.[22,23] Highly crosslinked polymeric nanohydrogels have the disadvantage of low biodegradability and are often prepared by radical initiators or metallic catalysts, which are incompatible with most molecules of interest for encapsulation. In those cases, the drug loading is usually made post-gelification, depending on the drug diffusion, and swellability of the hydrogel. To minimize these problems of nanohydrogels for nanomedicine applications, our group has developed a new Laponite-based nanohydrogel formulation that is nonswellable and can be gelified in presence of a wide variety of chemically sensitive molecules. Moreover, we have demonstrated that these nanohydrogels can be used as pH-responsive biodegradable nanocarriers,[20] because Laponite degrade into nontoxic species at pH lower than 7.0.[4]

1.2.1 Drug delivery systems against cancer diseases

Unlike healthy cells, cancer cells grow and multiply uncontrollably changing the microenvironment, invading nearby areas, and spreading to other areas of the body through some ways, like by the blood vessels and by the lymphatic system.[24]

The changes in the tumor microenvironment (TME) are one way of many to be explored as route to treat and suppress the cancer growth. Once the endothelial cells in a tumor vessel have loose interconnections and focal intercellular openings,[25] the vascular pore sizes become larger (20-800 nm) compared to normal tissue (5-10 nm) [26], and the barrier function is affected[27] allowing the passage and accumulation of materials with a size larger than 20 nm.[28] This difference in the intercellular opening can be used to selectively accumulate nanomaterials into tumor tissues, the so-called enhance permeation and retention effect (EPR) (Figure 3a).The EPR effect is also called passive targeting, in which the nanoparticles pass through the leaky vasculature and accumulate in the tumor cells rather than in healthy cells. Another type of selectivity towards tumor cells relies on biological interaction between ligands functionalized on the surface of nanoparticles (that can be proteins, polysaccharides, nucleic acids and small molecules) and specific receptors that are overexpressed in cancer cells (Figure 3b).[29]

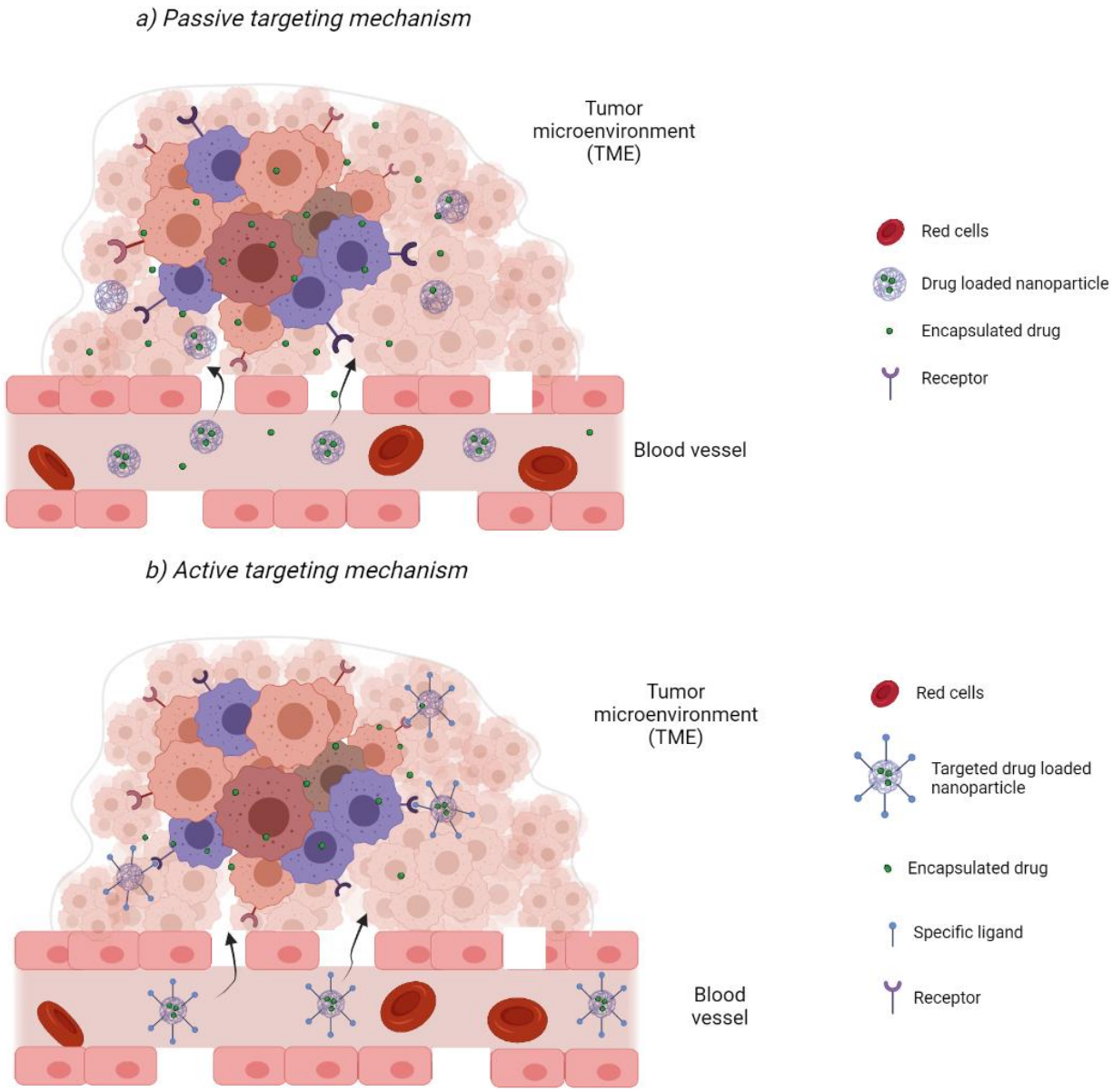

Figure 3. Scheme illustrating the mechanisms to deliver drugs into the cancer cells by nanoparticles: a) the passive targeting and b) the active targeting mechanisms.

Based on this, stimuli-responsive nanoparticles can be used as drug delivery systems to encapsulate small drugs, prevent their early degradation, and release the drugs at the target site through external stimuli, such as temperature changes,[30] or internal stimuli like pH changes.[31] Nanomaterials that respond to pH variations, like Laponite-based nanohydrogel, can be deformed or degraded under changes in the surrounding pH, and are interesting species to be used in the treatment of cancer, since the tumor microenvironment (TME) and inflammatory sites have pH significantly lower than the surrounding healthy tissue, i.e., values as low as 5.6 and in the range of 6.4-7 for tumors (according to some specific areas), in contrast to values of 7.3-7.4 for normal tissues.[32]

1.2.2 Co-delivery of anticancer drugs

Comparing to the single-drug approach, the combination strategy of different anticancer drugs has been studied with the aim of increasing the anticancer effects of the drugs and/or reducing the resistance that can occur when using the same drug over the long term.[33] When two or more drugs are combined, there are three possible outcomes: antagonism, when occurs adverse interaction between drugs that leads to decreased efficiency; additivity, with no positive interaction between the drugs and, consequently, no general beneficial effect; and synergism, in which the effects of drugs amplify each other's, resulting in an higher efficiency than the simple sum of the both drugs effect.[34] The level of interaction between anticancer drugs can be quantitatively calculated based on methods such as Chou and Talalay's Combination Index (CI). The CI for the drug combination is considered as synergistic when CI<0.9, antagonistic to CI>1.1, and just additive if CI = 0.9 to 1.1.[35] A basic approach to obtain these values for n drugs can be done by the Equation 1.[35]

$$CI = \sum_{N=1}^{n} \frac{(D_{comb.,N})}{(D_{alone.,N})} \qquad \text{Eq. 1}$$

where $D_{comb,N}$ is the dose of drug N in combination with others and $D_{alone,N}$ is the dose of the drug N when used alone.

Cisplatin, 5-Fluorouracil and Cyclophosphamide are important drugs in currently used in chemotherapy treatments for a variety of cancer types. Cisplatin (CP), a metal-based chemotherapeutic drug, was approved by the Food and Drug Administration since 1978 and has been used for the treatment of several cancers such as ovarian, cervical, breast and head either alone or in combination with other drugs.[36] Its antitumor activity is believed to be related to its interaction with DNA (genomic or mitochondrial), creating lesions, blocking the production of proteins, interfering in DNA replication and finally leading to apoptosis.[37] However, sometimes cisplatin does not act in its highest potential due to the side effects in the patient and the drug resistance that can arise. One way to improve these disadvantages is to use the cisplatin in combination with other drugs like 5-Fluorouracil and Cyclophosphamide, which was investigated by Dimery and co-workers (1990).[38] 5-Fluorouracil, a pyrimidine derivative, has also been used for a long time, its mode of action is probably the inhibition of thymidylate synthase (TS), a critical enzyme for DNA replication and cell growth, by fluorodeoxyuridine monophosphate (FdUMP) metabolite.[39] Cyclophosphamide is an alkylating cytotoxic drug used for a broad range of cancers, and its metabolized by the liver enzymes resulting in an active metabolite that interacts with DNA, inhibiting DNA replication and causing cell apoptosis.[40]

Based on all the considerations presented so far, this work aims to develop two nanostructured materials for two different applications: i) Laponite-based hydrogels with *in situ* synthesized gold, silver, platinum and palladium nanoparticles to be used as heterogeneous catalysts, and ii) Laponite-based nanohydrogels with anticancer drugs co-encapsulated to be applied against two cancer cell lines (MCF-7 and HeLa), and study the combination effect of the drugs against the cancer cells.

2. METHODOLOGY

2.1 Materials

The Laponite XLG was obtained from Southern Clay Products and the following materials were purchased from Sigma-Aldrich: Sodium polyacrylate (SPA) (5 KDa, M_w ~5,100 by Gel Permeation Chromatography), Tetrachloroauric(III) acid ($HAuCl_4$), Silver nitrate ($AgNO_3$), Potassium tetrachloroplatinate(II) (K_2PtCl_4), Potassium tetrachloropalladate(II) (K_2PdCl_4), 4-nitrophenol (4-NP), Sodium borohydride ($NaBH_4$), SPAN®85, Cyclohexane, cis-Diammineplatinum(II) dichloride (Cisplatin), 5-Fluorouracil, Cyclophosphamide monohydrate, and WST-8 assay. RPMI-1640 medium, Dulbecco's modified Phosphate-buffered saline (DMPBS, pH 7.4), and fetal bovine serum (FBS) were purchased from Cultilab Materiais Para Cultura de Células LTDA (Campinas, SP, Brazil). Dulbecco's modified Eagle's medium (DMEM) was purchased from Nutricell Nutrientes Celulares (Campinas, SP, Brazil). Trypsin-ethylenediaminetetraacetic acid solution (Trypsin-EDTA) was obtained from Gibco. Phosphate buffer solution (PBS) was prepared using only sodium and potassium salts, and NaOH and/or HCl to adjust pH (pH 7.4).

2.2 Synthesis of metallic nanoparticles (M NPs) into hydrogels (HG)

The metallic nanoparticles were synthesized *in situ* in the hydrogels with no addition of external reducing agents. The hydrogels were made based on methodology developed in our group (Becher *et al.* 2019).[4] To form the hydrogels, 1mL of Laponite solution (500 mg of Laponite and 10 mg of sodium polyacrylate dissolved in 10 mL of deionized water) was placed in a 3 mL polystyrene vial under agitation (1000 rpm), at 25 °C. Then, to later form the metallic nanoparticles, 100 µL of gold, silver, platinum, or palladium salts aqueous solution with variable concentration was added to the vial containing the Laponite nanodiscs and polyacrylate and the agitation was immediately increased to 2000 rpm. After 2 min, the solutions were already gellified, and the nanoparticles were formed *in situ* after a variable time (hours or days). The materials were named as "HG@M", indicating the hydrogel with metallic M nanoparticle, synthesized at 25 °C.

The blank hydrogel was prepared using the same procedure described above, but 100 µL of 1.0 M PBS solution was added instead of the metal salts solutions.

2.2.1 Characterization

2.2.1.1 Ultraviolet-visible spectroscopy (UV-Vis)

The *in situ* formation of nanoparticles into the hydrogels were evaluated firstly by UV-vis absorption spectra with a 1 mm polystyrene cuvette at room temperature using a UV-vis Agilent HP8453 spectrometer. For this analysis, the hydrogels were prepared directly inside the cuvettes instead of the 3 mL vials.

2.2.1.2 Fourier Transform Infrared spectroscopy (FTIR)

Fourier transform infrared (FTIR) spectroscopy was done for hydrogels using Agilent Cary 630 FTIR spectrometer with a spectral range of 4000-400 cm^{-1} and resolution of 2 cm^{-1}, and the measurements were carried out by placing the samples directly on the diamond ATR sensor.

2.2.1.3 Rheology

Rheology was used to observe the mechanical properties of these synthesized hydrogels and the measurements were carried out in a Haake RheoStress RS1 rheometer. The materials were tested with amplitude sweep (strain sweep, SST) to study the response of material against an increasing deformation amplitude (strain, γ) and obtain information of some parameters such as the linear range of viscoelasticity (LRV), storage modulus (G') and loss modulus (G''), at constant frequency (1 Hz) and temperature (25 °C).

2.2.1.4 Transmission Electronic Microscopy (TEM)

To confirm the presence and analyze the size and morphology of the nanoparticles into hydrogel, microscopy analyze was done by Transmission Electronic Microscopy (TEM JEM1400PLUS (Jeol, Japan) operating at 120 kv, where the sample was dried directly on carbon-coated copper grid.

2.2.2 Reductive catalytic properties

The catalytic activity of AuNPs, AgNPs and PtNPs were tested using one model reaction based on the catalytic reduction of 4-nitrophenol (4-NP) by borohydride ions (BH_4^-) in the presence of the metallic catalyst.[41]

The procedure to study the reductive catalytic activity of the nanoparticles into the hydrogels was adapted from Haraguchi (2014).[13] with few modifications. In a quartz cell, 0.5 mL of $NaBH_4$ solution (17 mM) was added to 2 mL of 4-nitrophenol solution (0.16 mM). Then, variable amounts of HG@Au, HG@Ag, and HG@Pt were subsequently added. The UV-vis spectra of the reaction mixture were collected immediately with 1 min intervals, for 20 min, at 25 °C.

The conversion (%) of 4-NP to 4-AP was calculated based in the UV-vis absorbance of 4-nitrophenolate ion by the following equation (Equation 2):

$$Yield\ of\ reduction\ (\%) = \frac{(A_0 - A_t)}{A_0} x\ 100 \qquad \text{Eq. 2}$$

where A_0 is the initial absorbance of 4-nitrophenolate ion (at 400 nm)[41] after the addition of $NaBH_4$; and A_t is the absorbance of this ion over the time, at same wavelength.

2.3 Synthesis of Nanohydrogels (NH)

The nanohydrogels were synthesized by inverse miniemulsion technique and were based on a methodology developed by our group[20] with few modifications (Figure 4). For all nanomaterials, to the organic phase formed by 8 mL of cyclohexane and 75 mg of SPAN85, was added the aqueous phase consisting of 500 µL of Laponite aqueous solution previously prepared with the ratio 100:1 of Laponite nanodiscs:sodium poly(acrylate) (SPA) and 500 µL of drug aqueous solution (Cisplatin, 5-Fluorouracil or Cyclophosphamide, and in some cases, different mixing ratios between these drug solutions were used). The mixture was ultrasonicated, in an ice bath, twice (Branson Sonifier 450 Digital, 0.5 inch tip) for 6 min with 50% of amplitude and at a pulse regime of 0.9 s of sonication intercalated with 0.3 s of pause, and between the ultrasound runs, 100 µL of 1.0 M phosphate buffer solution (PBS) was added, finally forming the nanohydrogels **NHCP**, **NHFU** and **NHCPA** (nanohydrogel with Cisplatin, 5-Fluorouracil and Cyclophosphamide, respectively) and it combination: **NHFUCP** for nanohydrogel with 5-Fluorouracil and Cisplatin co-encapsulated, and **NHCPCPA** for nanohydrogel with Cisplatin and Cyclophosphamide. Intending to a more stable storage, after

evaporation of organic solvent, an aliquot of each nanohydrogel synthesized was dispersed into 10 mL of a 0.1 M PBS (pH 7.4), and the final dispersion was stored in the fridge.

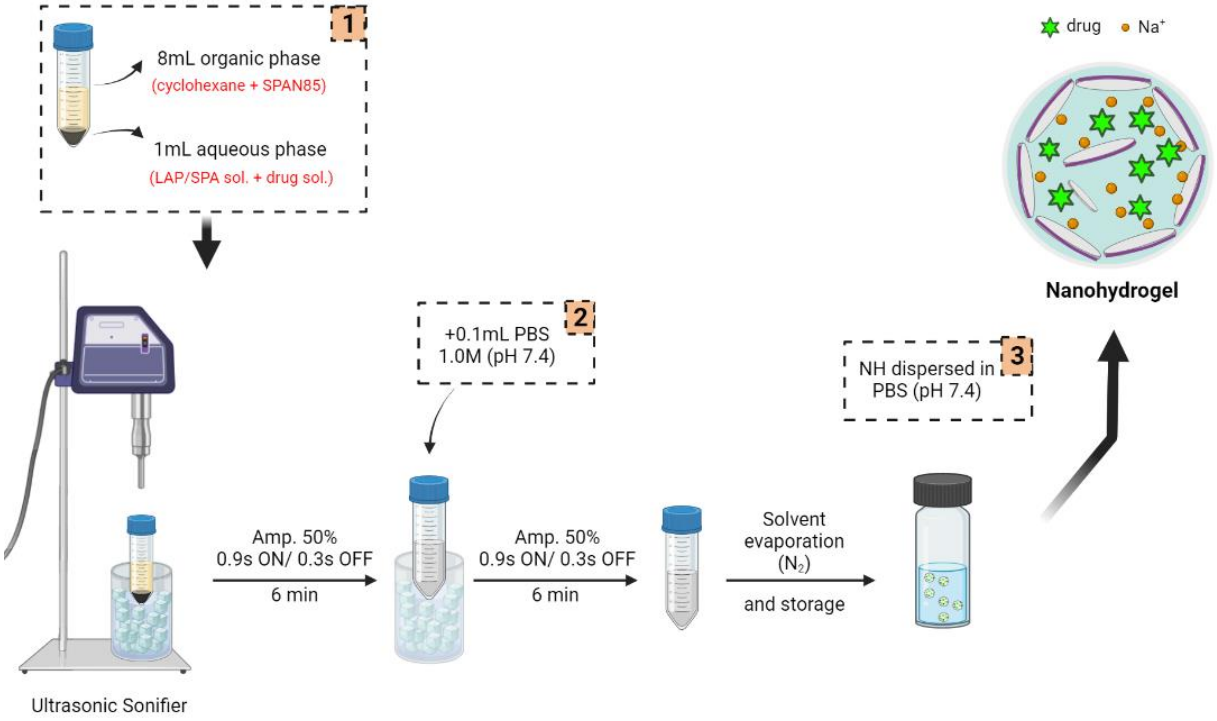

Figure 4. Schematic representation of the synthesis of the nanohydrogels using miniemulsion technique.

2.3.1 Characterization of nanohydrogels by Dynamic Light Scattering

The average size and zeta potential of nanohydrogels were obtained by dynamic light scattering using a Malvern Zetasizer Nano ZS-Zen3600 equiped with a 4 mW He-Ne laser, light wavelength of 632.8 nm, and detection at scattering angle of 173°. All measurements were done at 25 °C using a disposable capillary cell (DTS1070). The samples were analyzed as dilutions (10000x in PBS pH 7.4), and three measurements were taken of the resulting dilutions. The results are presented in percentage by number of particles, as mean ± standard deviation (SD).

2.3.2 Stability study

The stability of nanohydrogels was evaluated by monitoring the changes in their size over time. The measurements were obtained by dynamic light scattering using a Malvern Zetasizer Nano ZS-Zen3600 equiped with a 4 mW He-Ne laser, light wavelength of 632.8 nm,

and detection at scattering angle of 173°. Nanohydrogels were dispersed in acetate buffer solution (dilutions 10000x, pH 5.44), at 37 °C, and three measurements were taken of the resulting dilutions.

2.3.3 Cell viability

The human breast adenocarcinoma cells (MCF-7, ATCC® HTB-22) were grown in RPMI-1640 culture medium supplemented with 10% fetal bovine serum (FBS) and antibiotics (penicillin at 100mU mL^{-1} and streptomycin at 100 µg mL^{-1}). The human cervix adenocarcinoma cells (HeLa, ATCC® CCL-2) were cultured in Dulbecco's modified Eagle's medium with high glicose supplemented with 10% FBS, 1% nonessential amino acids (NEAA), and antibiotics (penicillin at 100mU mL^{-1} and streptomycin at 100 µg mL^{-1}). All the cell lines were maintained in T-75 cm^2 cell culture flasks with 12 mL of medium, at 37 °C, in a humidified atmosphere with a controlled percentage of CO_2 (5% CO_2) and at every 2-3 days the culture medium was refreshed, and when the cells from culture flask reached 70-80% confluency, the cells were detached and plated into a new treated T-75 cm^2 cell culture flask with 12 mL of medium. To be used in the tests, cells were seeded into 96-well plates at a cell density of 7.5 x 10^3 cells per well and incubated for 24 h to ensure cell adhesion in the plates before any treatment. Then, the medium was replaced by a fresh one with different concentrations of nanohydrogels (final volume of 200 µL per well), and the plates were incubated for 48h under the same conditions. After this period, the cellular viability was quantified by colorimetric method using the CCK-8 (Cell Counting Kit-8) and the absorbance of the solution in each well was measured at 450nm using FlashScan 530 Analytik Jena.

3. RESULTS AND DISCUSSION

3.1 Laponite-based hydrogels with metallic nanoparticles for catalysis

In order to study the *in situ* formation of metal nanoparticles in the hydrogel matrix, metal salts were used as crosslinkers for the gelification of hydrogels using the procedure previously developed in our group for Laponite-based hydrogel formation with other types of salts[4]. When Laponite was dispersed in deionized water under magnetic stirring, the interlayer Na^+ ions started to exfoliate, and the early cloudy dispersion slowly evolved into highly viscous materials like a hydrogel.[4] With the addition of sodium polyacrylate (SPA), the cloudy dispersion became homogenous once the negative SPA wrap the positively edges of the nanodiscs, increasing the rate of exfoliation.[4] This interaction is confirmed by zeta potential of diluted Laponite/SPA solution, as seen in Figure 5a, which showed an increased negative value as a consequence of the exposure of negative surface of Laponite nanodiscs once the polymer wrapped around nanodisc's edges, neutralizing the positive charges.[20] Moreover, the DLS data (Figure 5b) for Laponite nanodiscs and Lap/SPA solution did not show any significant difference in the average size, suggesting that most polymer chains interact with only one nanodisc. If the polyacrylate chains worked as a bridge between several nanodiscs would expect a significant increase in the size of system due to the entangled nanodiscs.

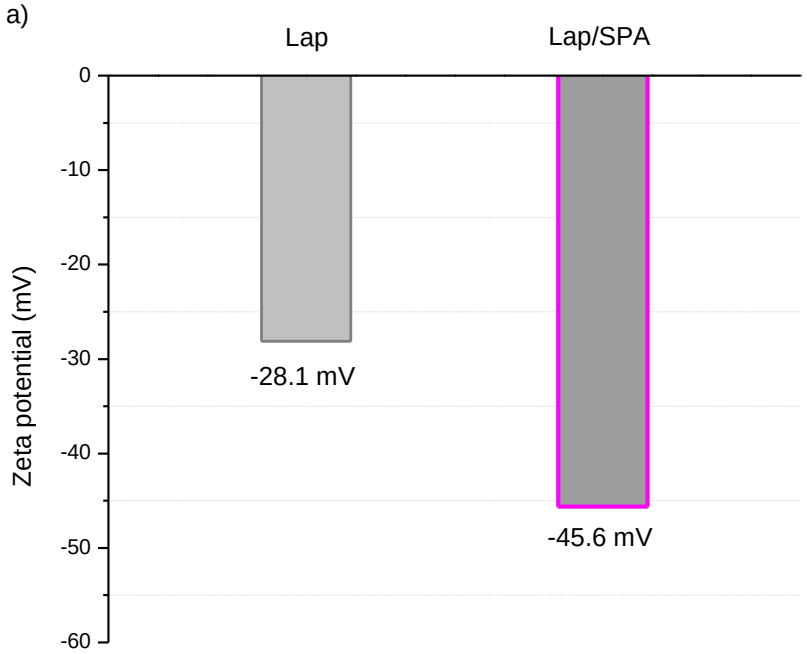

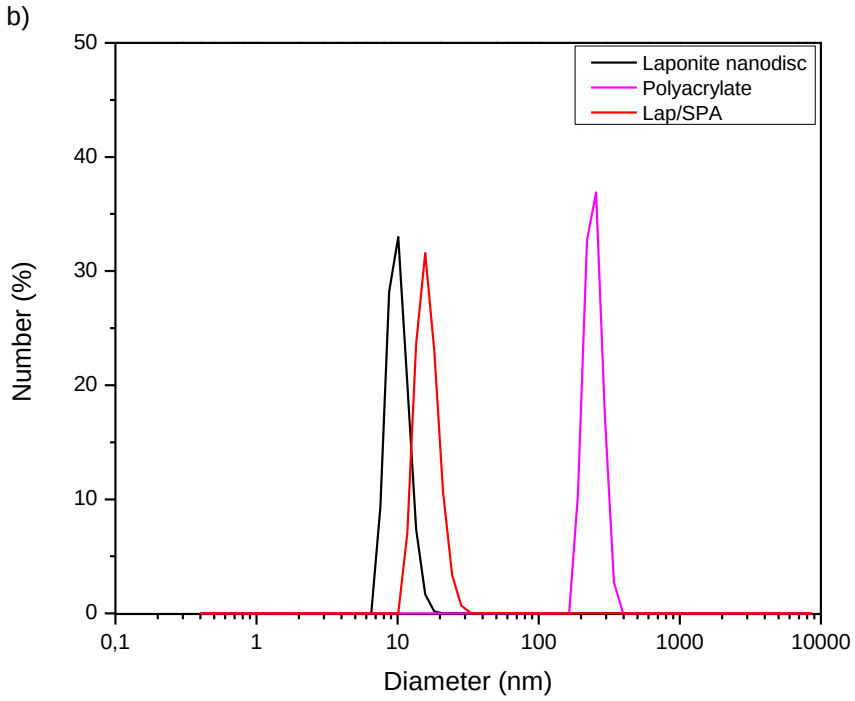

Figure 5. a) Zeta potential data obtained for nanodiscs and Laponite/SPA solution (nanodisc's edges wrapped by polyacrylate chains), and b) DLS data showing the size of nanodiscs, polyacrylate and Laponite/SPA solutions, with intensity represented by number (%).

After the solution become homogenous, an aliquot of the Laponite/SPA solution was transferred to a polystyrene cuvette and the metal salt solution was added to form the hydrogel. The evolution of the hydrogel color was followed visually (pictures of Figures 6-9) and by absorption spectroscopy to see the eventual formation of M^0 nanoparticles within the hydrogel network.

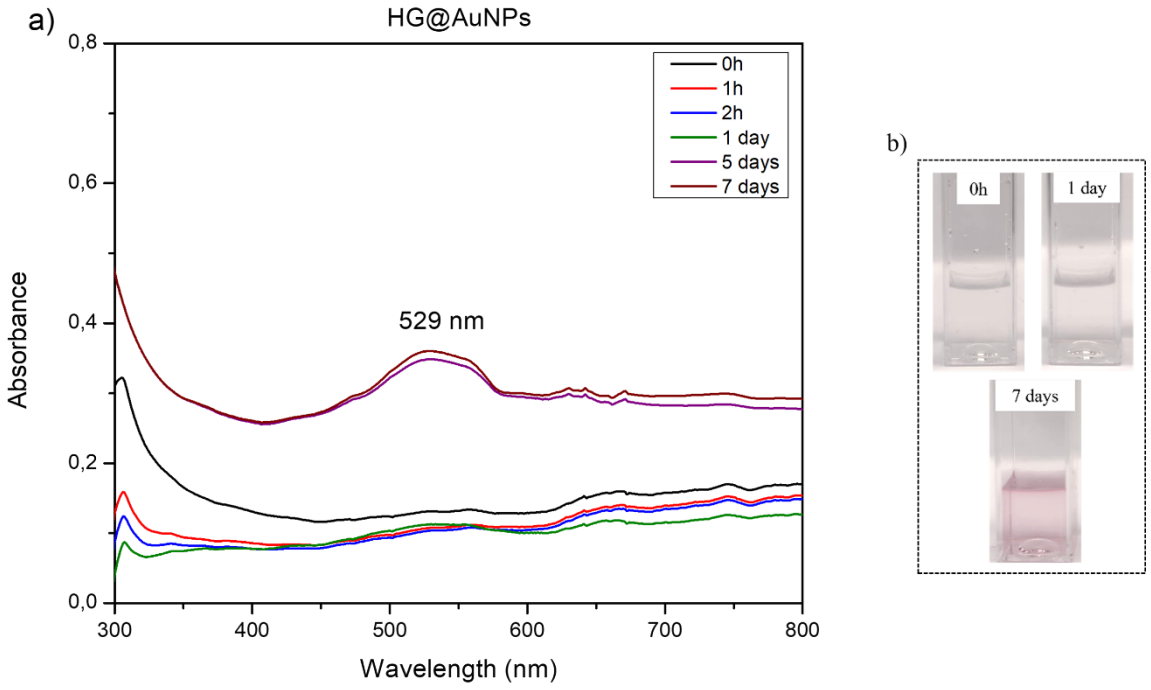

Figure 6. a) UV-vis absorption spectra of hydrogel formed with $HAuCl_4$ salt at different time points and b) color change of hydrogel with the formation of Au-NPs over time.

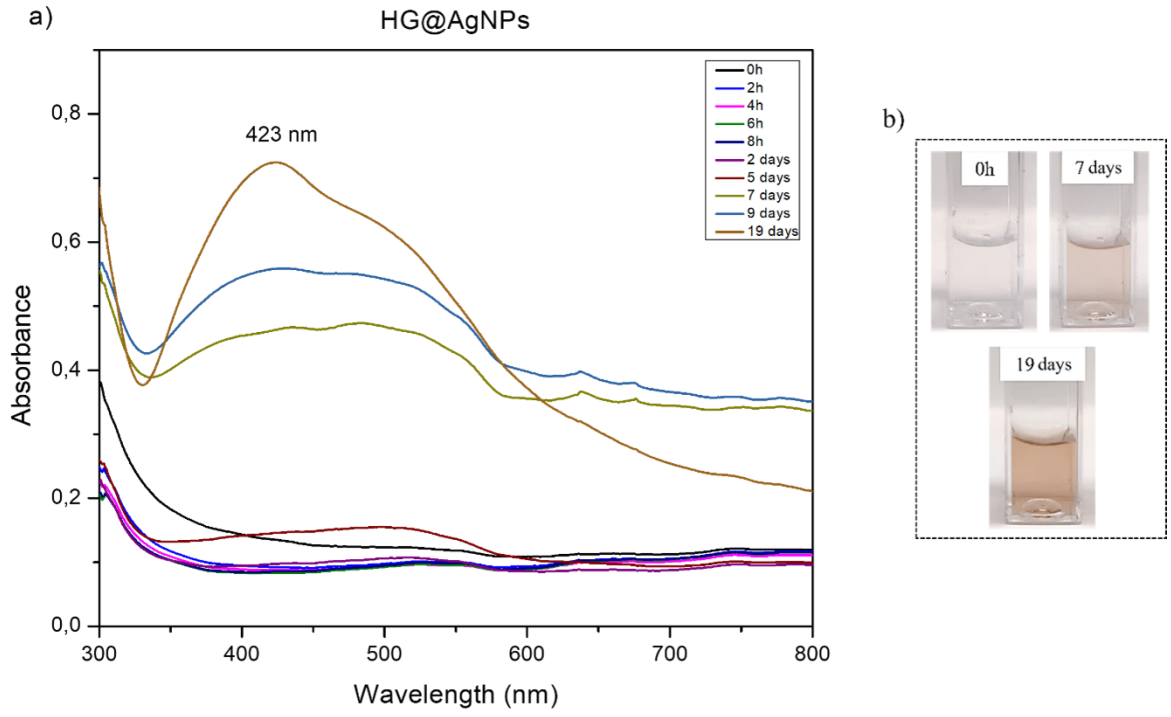

Figure 7.a) UV-vis absorption spectra of hydrogel formed with $AgNO_3$ salt at different time points and b) color change of hydrogel with the formation of Ag-NPs over time.

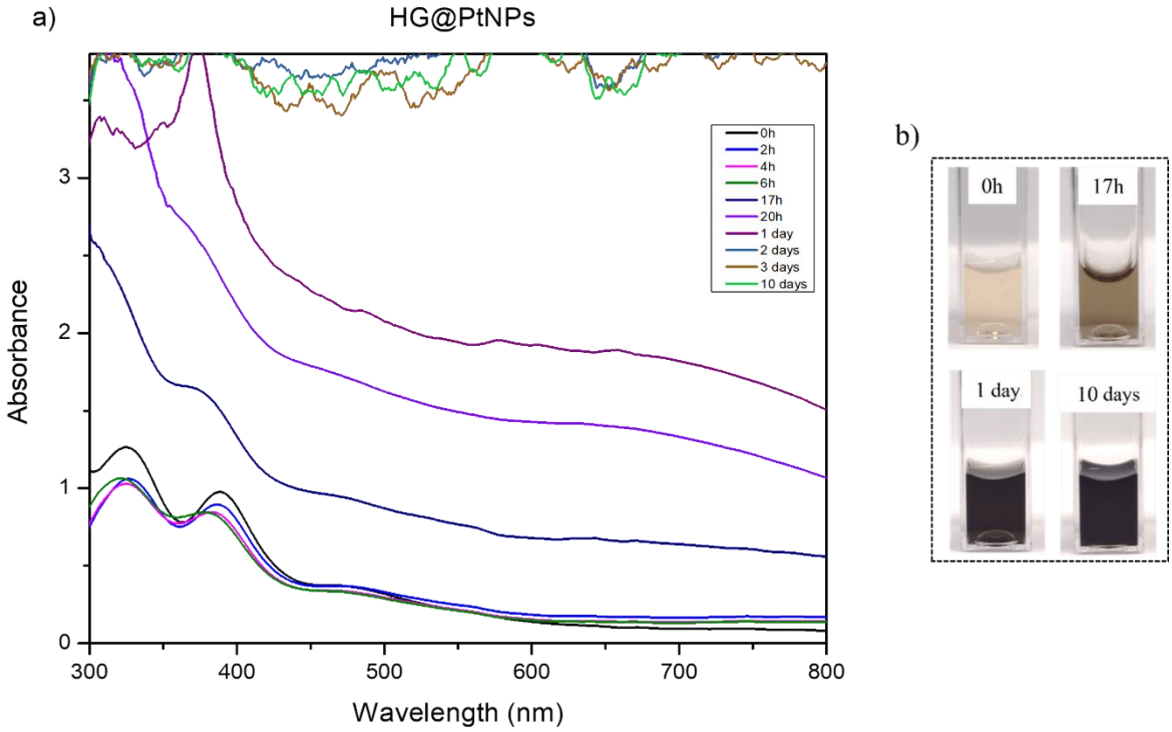

Figure 8.a) UV-vis absorption spectra of hydrogel formed with K_2PtCl_4 at different time points and b) color change of hydrogel with the formation of Pt-NPs over time.

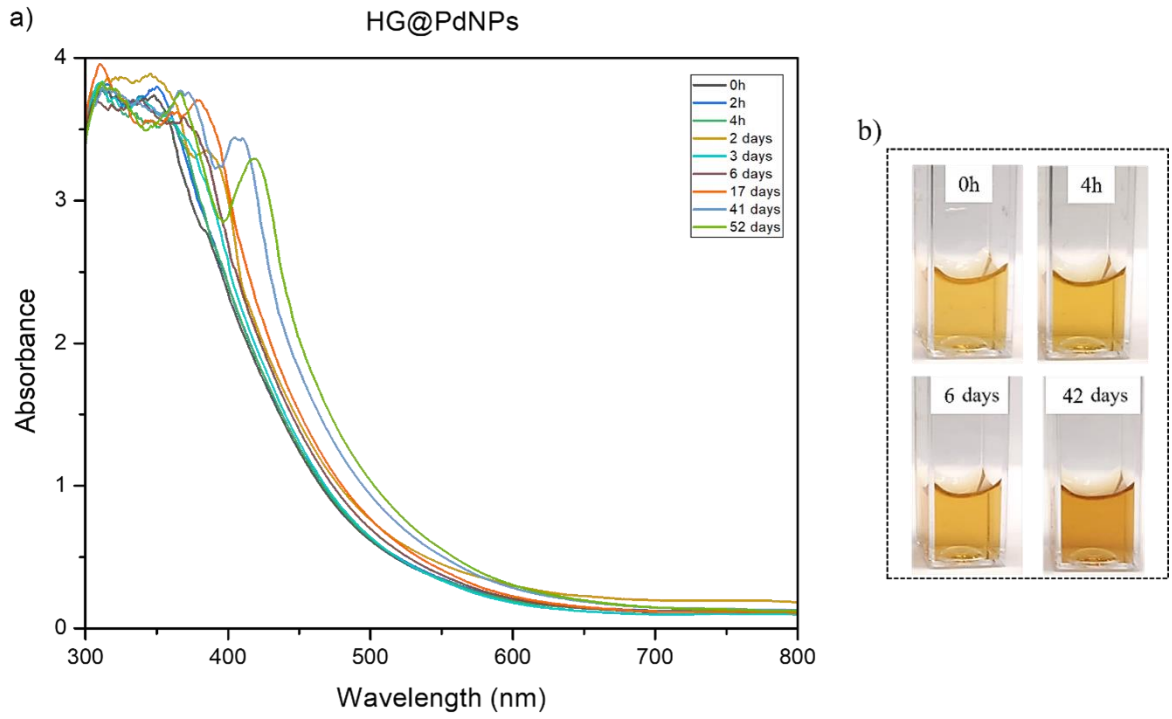

Figure 9.a) UV-vis absorption spectra of hydrogel formed with K_2PdCl_4 at different time points and b) color change of hydrogel over time.

As seen in Figure 6-9, the drastic color changes of the hydrogels are indicative of the *in situ* formation of their respective nanoparticles, which was accompanied by changes in the UV-vis spectrum: the new band around 530 nm as indicative of AuNPs (Figure 6a);[42] the broad band at 423 nm associated with AgNPs (Figure 7a);[43] and the disapearance of bands at 325 and 388 nm which are characteristic of the K_2PtCl_4 solution, as indicative of the reduction of Pt(II) to Pt over the time, forming PtNPs (Figure 8a).[44] In the case of HG@Pd (Figure 9), however, it is not possible to indicate the formation of PdNPs based on the color since no drastic color change was observed in the hydrogel and the UV-vis spectrum does not show big changes in the bands over time. For this case, TEM microscopy will be essential to observe the presence/absence of Pd nanoparticles.

The *in situ* formation of these metallic nanoparticles is probably due to the interaction of the metal ions with the exfoliated clay nanodiscs in aqueous medium, more specifically, with the clay surface.[45] Since the surface of the Laponite is constituted by siloxane groups (Si-O) in the tetrahedral sheet, the metallic ions might interact with the Si-O forming a complex that, later, will be reduced on the clay surface possibly via successive proton-electron transfer processes. After several reductions, occurs the coalescence of M^0 atoms that form clusters of metallic atoms, and subsequently results in nanoparticles trapped on the hydrogel network. This hypothesis is supported by Haraguchi (2014), who did an *in situ* formation of Pt nanoparticles in a gel consisting of NIPA and Laponite without adding a reducing agent.[13] Moreover, the exfoliated clay nanodiscs of the hydrogels not only interact favorably to reduce the metallic ions of the solutions, but also act as support material for the formed nanoparticle, without their precipitation even after days, as observed in the hydrogel's photos (Figure 6b-8b).

The TEM images confirm the presence of spherical Pt NPs (Figure 10) and Ag NPs (Figure 11) with a diameter in range of 1-2 nm and 2-3 nm, respectively. The Figures 10 and 11 shows the nanoparticles trapped and well-dispersed on the hydrogel network, as expected in accordance with the explained hypothesis.

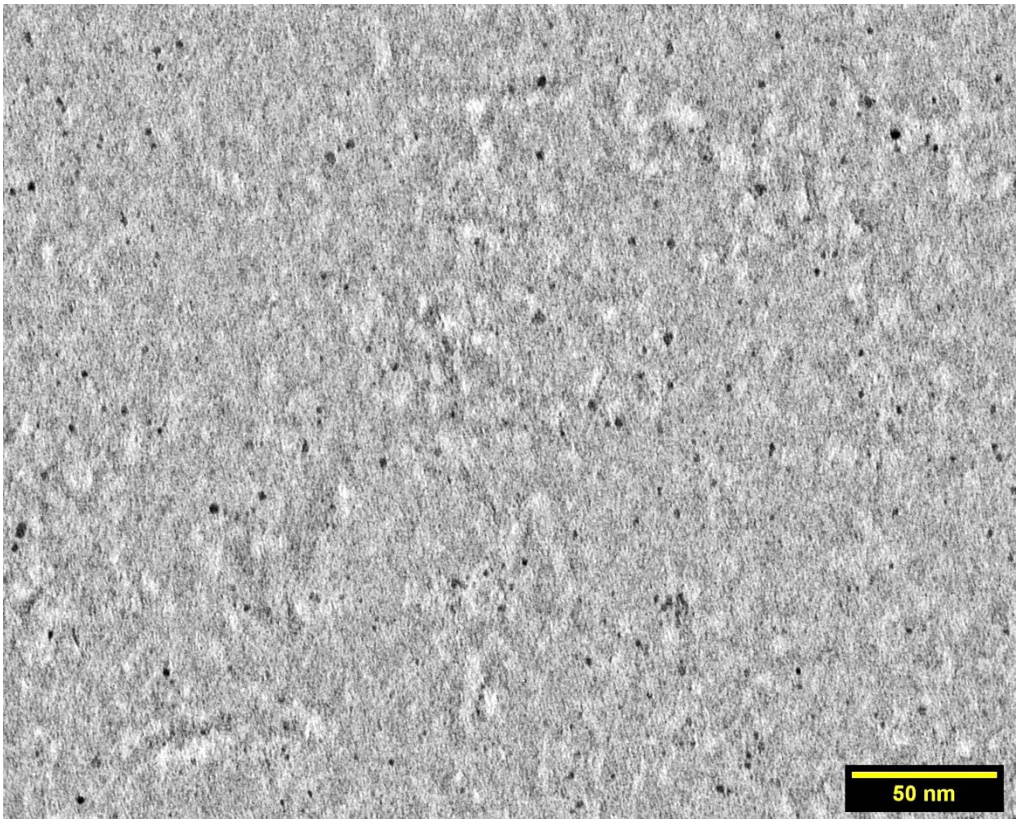

Figure 10. TEM images of Pt nanoparticles with a size range of 1-2 nm (black points in the images), from dried HG@Pt (synthesized at 25 °C).

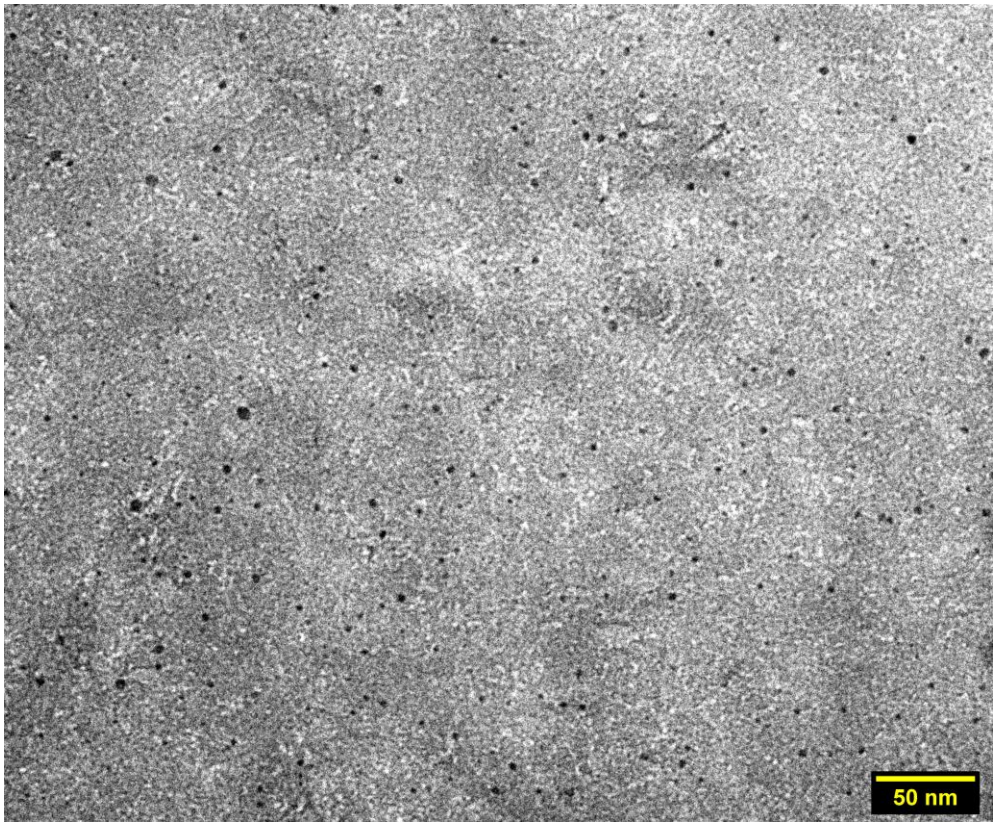

Figure 11. TEM images of Ag nanoparticles with a size range of 2-3 nm (black points in the images), from dried HG@Ag (synthesized at 25 °C).

The effect of temperature on the *in situ* formation of nanoparticles was studied by heating the resulting hydrogels at 40˚C. Just after gelification, the hydrogels were placed in a bath at 40 °C for 48h, and the eventual NPs formation was followed by color change of hydrogels and UV-Vis over time (Figures 12-14). The hydrogels synthesized by this way were named as "HG@M40", where M40 indicates the metal nanoparticles formed at 40 °C.

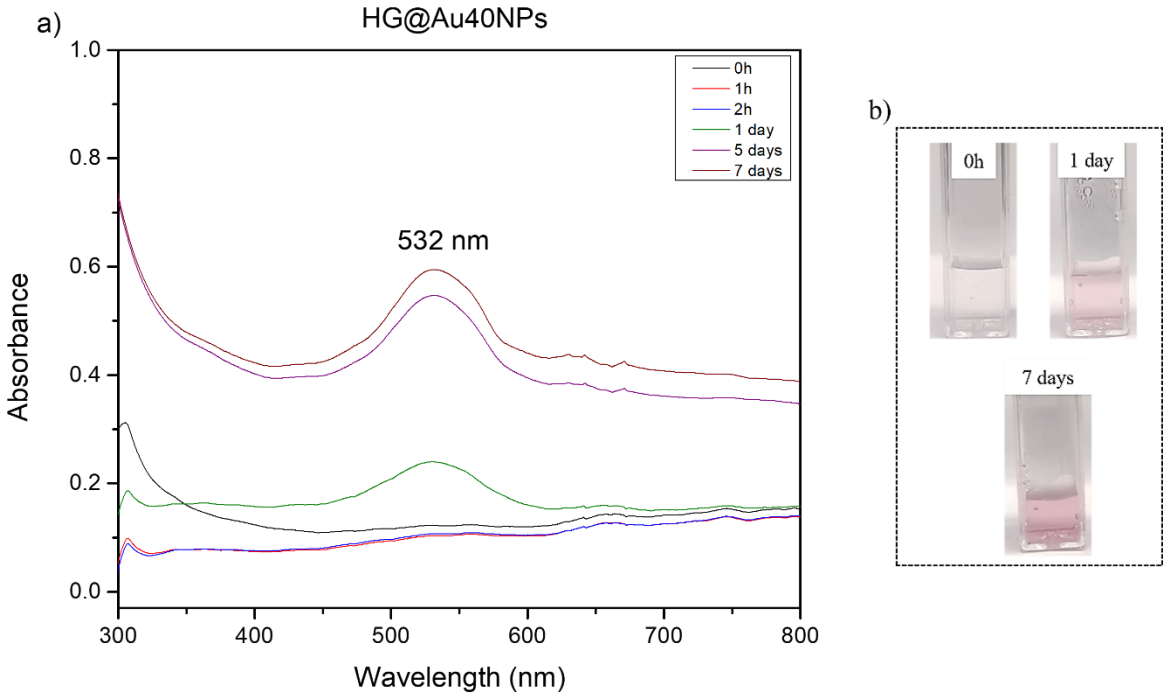

Figure 12. a) UV-vis absorption spectra of hydrogel formed with $HAuCl_4$ at different time points and b) color change of hydrogel with the formation of Au-NPs over time (at 40 °C over 48h).

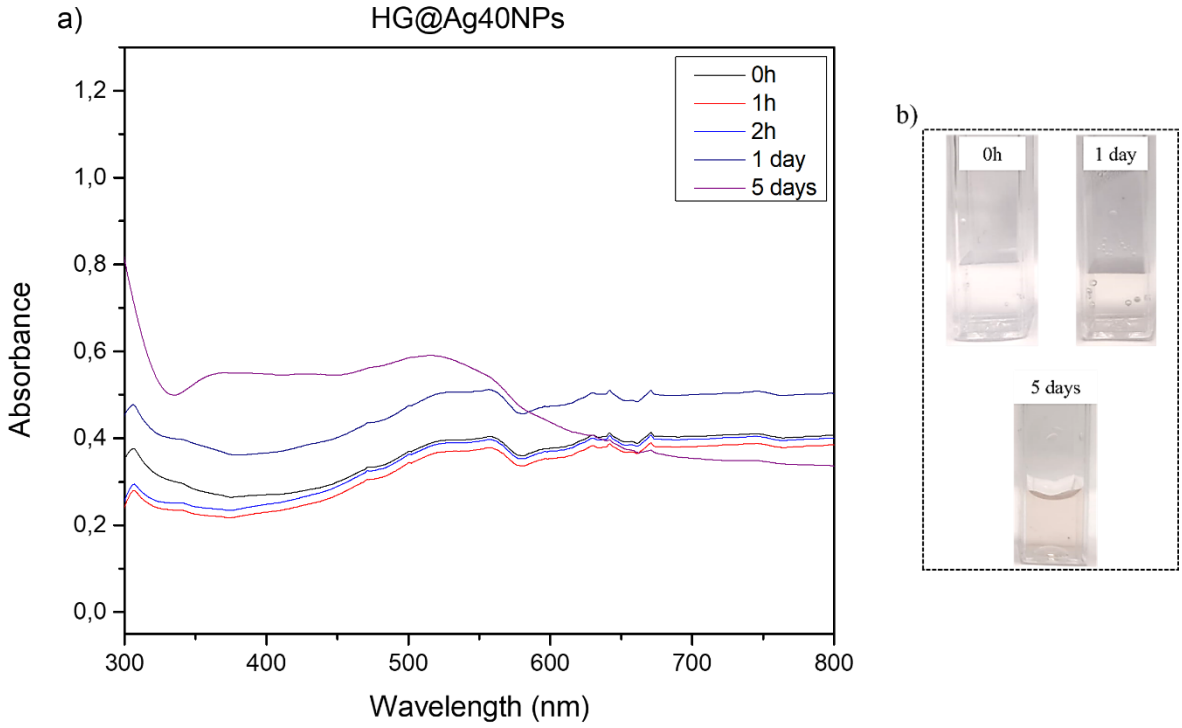

Figure 13. a) UV-vis absorption spectra of hydrogel with $AgNO_3$ salt at different time points, b) color change of hydrogel with the formation of Ag-NPs over time (at 40 °C over 48h).

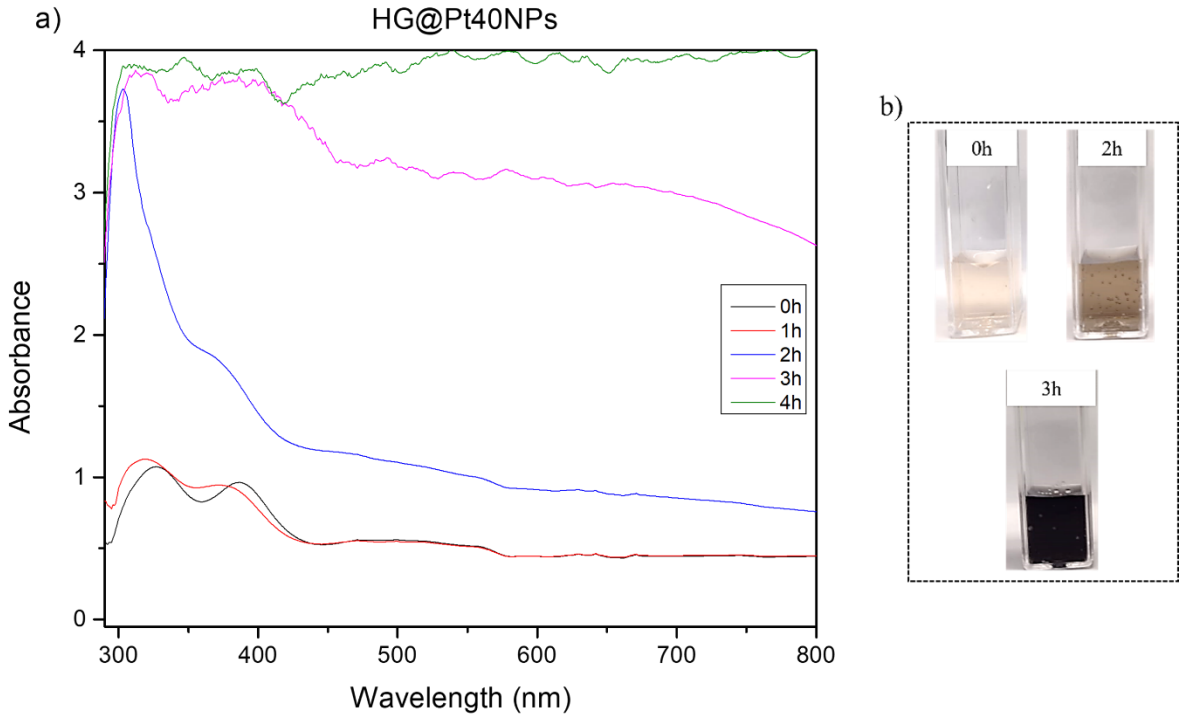

Figure 14. a) UV-vis absorption spectra of hydrogel formed with K_2PtCl_4 at different time points b) color change of hydrogel with the formation of Pt-NPs over time (at 40 °C over 48h).

As seen in Figure 12 and 14, the increased temperature was favorable for a rapid formation of AuNPs (with a new band at 532 nm just one day after synthesis) and PtNPs (with a loss in the characteristic bands of Pt^{2+} solution at 325 and 388nm) nanoparticles, respectively. At 25 °C, it is possible that the reduction of the Si-O-M complexes takes place slowly. However, when the hydrogels were placed in a bath at 40 °C, there was a significant increase in the rate of reduction. Similar results were also obtained by Haraguchi (2014) for the synthesis of PtNPs into a NIPA-Lap gel, at 60 °C.[13]

Liu *et al.* (2020) has demonstrated that under sufficient metallic ion precursors, high temperature is favorable to both nucleation and growth of nanoparticles, but once the rate of growth is increased, there is also an increase in the particle size, as demonstrated in their work with the size of Ag NPs synthesized at different temperatures (7.8 nm when formed at 70 °C and 17nm at 90 °C).[46] Following this demonstration, the UV-Vis spectra obtained here for hydrogels synthesized at 25 °C and 40 °C also can be indicative of a difference in the size of nanoparticles. For Au hydrogels, they had the characteristic band at distinct wavelength: 529 nm for HG@Au (Figure 6a) and 532 nm for HG@Au40 (Figure 12a), and due the localized surface plasmon resonance (LSPR) of gold nanoparticles, the peak absorbance wavelength is slightly red-shifted with a possible increase in the particle diameter.[47]

Based only in the UV-Vis spectra, it is not possible to conclude about the positive influence of temperature on the synthesis of AgNPs (HG@Ag40, Figure 13a) since there is still no pronounced band in the range of 420 nm when compared with the HG@Ag (Figure 7a). Due to this, for the next experiments, was considered only the HG@Au40 and HG@Pt40.

FTIR spectroscopy of the hydrogels synthesized at 25 °C was performed and the spectra obtained are shown in Figure 15. In the total spectrum (Figure 15a), is seen a large band at 3100-3700 cm^{-1} that frequently is reported as a consequence of overlapped bands: -OH stretching of hydroxyl groups on the lattice (in the range of 3500-3700 cm^{-1}, such as Si-OH, Mg-OH, Li-OH, and MgLi-OH), and -OH stretching vibrations of free H_2O (near 3400 cm^{-1}).[48] Similarly, the region at 1634-1637 cm^{-1} is related to H-OH bending mode vibration (from H_2O molecules). Shoulder peak at 1075 cm^{-1} is attributed to Si-O (non-bridging oxygen) vibration and higher peak at 1001 cm^{-1} to Si-O stretching vibrations of the external tetrahedral sheets of nanodiscs. Comparing the νSi-O vibration on the pure Laponite nanodiscs that is observed at 982 cm^{-1} (usually at 960-990 cm^{-1} [4,49]), for the hydrogels HG@M the same stretching is obtained shifted in higher wavenumber value at 1001-1002 cm^{-1}, and probably this change was

a consequence of interactions between metallic ions and silanol group to result, finally, in nanoparticles on the matrix of hydrogel.

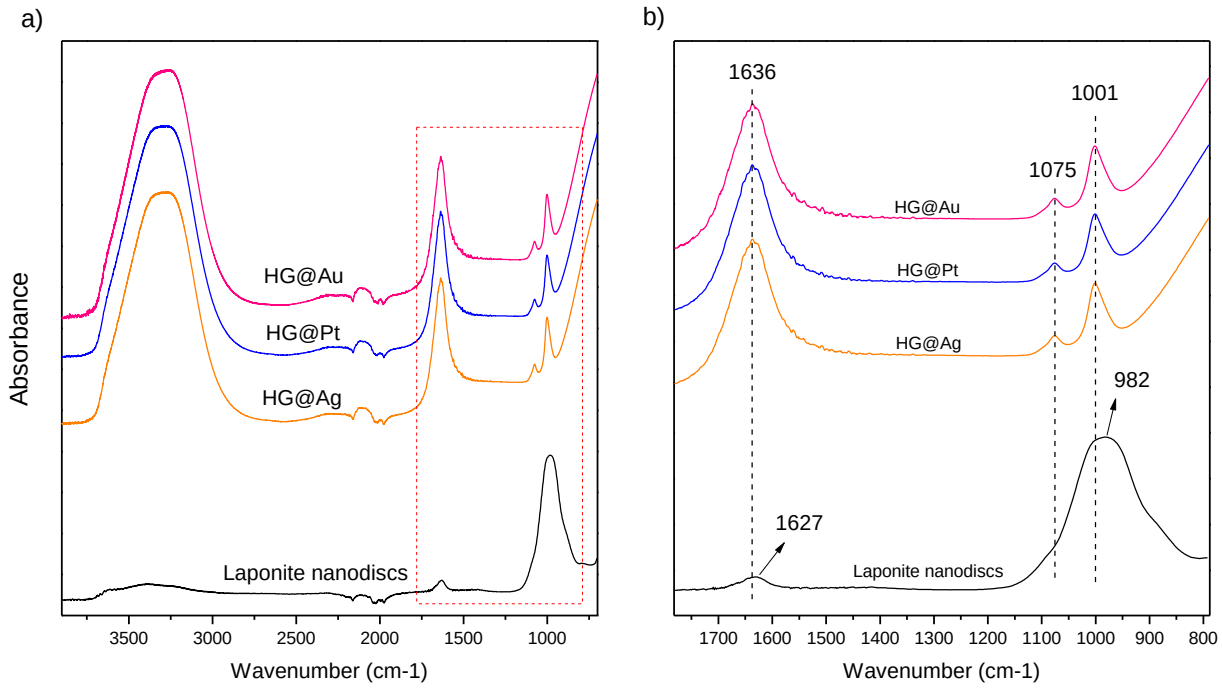

Figure 15. a) FTIR spectra of HG@AuNPs (-), HG@PtNPs (-), HG@AgNPs (-), and Laponite nanodiscs (-) as blank material, and b) region of spectra dashed in (a).

Intending to study the mechanical properties of the hydrogels was done rheological measurements and the results are presented in Figure 16.

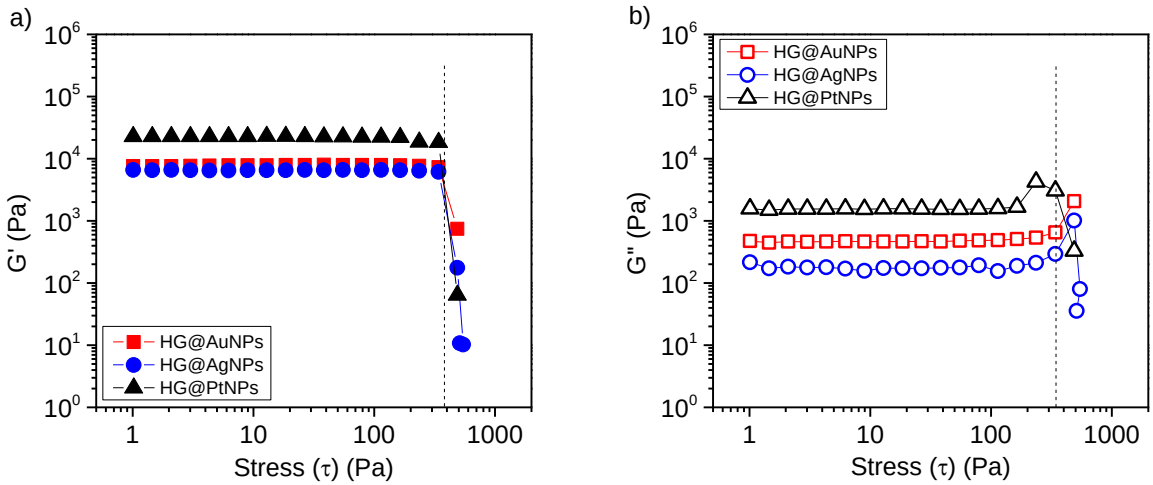

Figure 16. SST data obtained for hydrogels synthesized at 25 °C with Au, Ag and Pt nanoparticles, at 25 °C and constant frequency of 1 Hz. Comparative between the hydrogels of (a) storage modulus G', and (b) loss modulus G''.

As seen in the Figure 16a-b, at the begin of the stress sweep test, all hydrogels have G' higher than G'' under stress ranging from 1 to 340 Pa (indicated by dashed line), meaning that the elastic portion was dominant in all materials at that range and the confirming the gel-like behavior of these hydrogels [50]. Also, this range represents the linear range of viscoelasticity (LRV), which is the region where a stress can be applied without destroying the structure of the samples. The maximum G' values obtained by rheology for these three hydrogels were: $6.5x10^3$ Pa for HG@AgNPs, $7.9x10^3$ Pa for HG@AuNPs, and $2.3x10^4$ Pa for HG@PtNPs. Between the three hydrogels, the one with Pt NPs have a higher G' and G'' values which means that this hydrogel is stronger structurally than others.

The Figure 16b shows the relation of G'' (loss modules) for hydrogels and specifically in respect do HG@PtNPs, it is clearly observed that in a stress at 236 Pa there is a little increase in the viscous modulus (G'') with a subsequently decrease, probably due micro cracks in the structure of hydrogels as indicative of starting the breakdown until the maximum is reached with a macro crack, where G'' curves pass the G' curves (Figure 17). The cross-point between G' and G'' curves for the materials occurs at a stress of 436, 429 and 410 Pa for HG with Au, Ag and PtNPs, respectively. Higher than this stress values, the viscous nature (quasi-liquid state) of each hydrogel is prevailing over the elastic nature (quasi-solid state) [51].

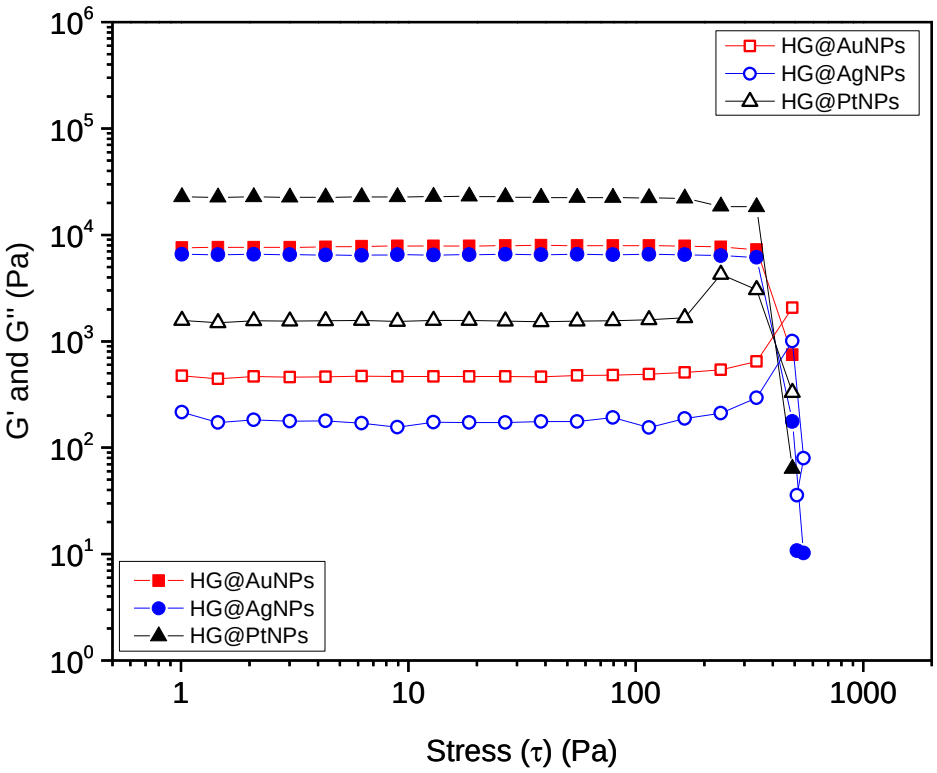

Figure 17. Comparative SST data between storage (G') and loss (G'') modulus, obtained for hydrogels synthesized at 25 °C with Au, Ag and Pt nanoparticles, at 25 °C and constant frequency of 1 Hz.

To study the applicability of HG@M hydrogels as catalysts, reduction of 4-nitrophenol (4-NP) to 4-aminophenol (4-NP) by sodium borohydride ($NaBH_4$) was used as a model reaction, because this reaction can be easily monitored by UV-vis. This reaction, although it is thermodynamically favorable, it is kinetically restricted in absence of a catalyst (as seen in the Figure 18) due to the high kinetic barrier between the repelling negative ions of *p*-NP and BH_4^-.[12,52] Furthermore, 4-NP is used to manufacture drugs, insecticides, and dyes, but it is toxic and has been classified as a priority pollutant by US Environmental Protection Agency (EPA), being carcinogenic and causing skin diseases.[53] On the other hand, the reaction product, 4-aminophenol (4-AP), is an important intermediate in the production of analgesics like paracetamol.[54]

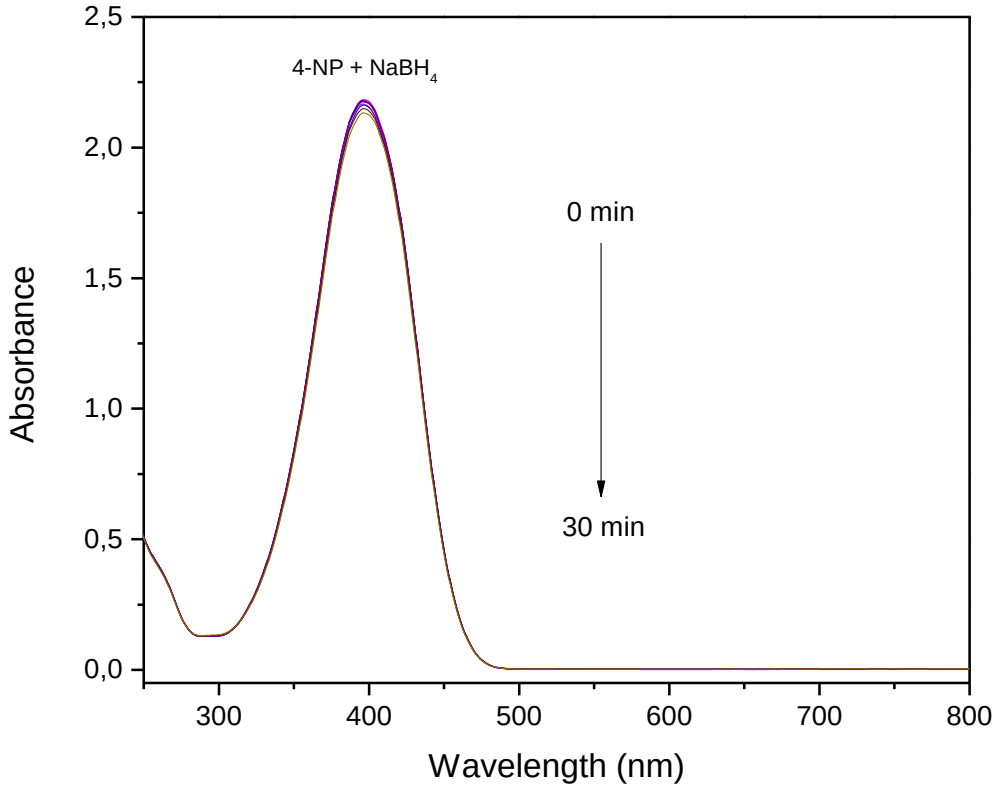

Figure 18. UV-vis spectra for reduction of 4-NP (0.16 mM) by NaBH4 (20 mM) without catalysts, over 30 min, at 25 °C.

The kinetic reduction experiment was performed at 25 °C using each HG@M as catalyst with three different amounts of hydrogels (100 mg, 200 mg and 300 mg of each hydrogel), and according to the UV-vis spectra obtained, % conversion of 4-NP to 4-AP was calculated following the Equation 2. The results for all catalysts used are presented in Table 1 and to calculate the kinetic rate constant was choose the best HG@M according to your yield of reduction. The amount of metallic nanoparticle was calculated as % mols of metal in the hydrogel related to the mols of 4-NP used. The Figures 19-21 show the reduction spectra specifically for those hydrogels that showed better catalytic activity.

Table 1. %Conversion of 4-nitrophenolate ion with the formation of 4-AP at variable amounts of metallic nanoparticles as catalyst (into hydrogels). Values were calculated based on the absorbance at 400 nm, with the reaction occurring for 20 min at 25 °C.

Catalyst	M^0 used (%)	Yield of reduction (%)
Au	69	99
	50	82
	26	42
Pt	107	84
	70	26
	39	16
Ag	172	93
	108	94
	52	97

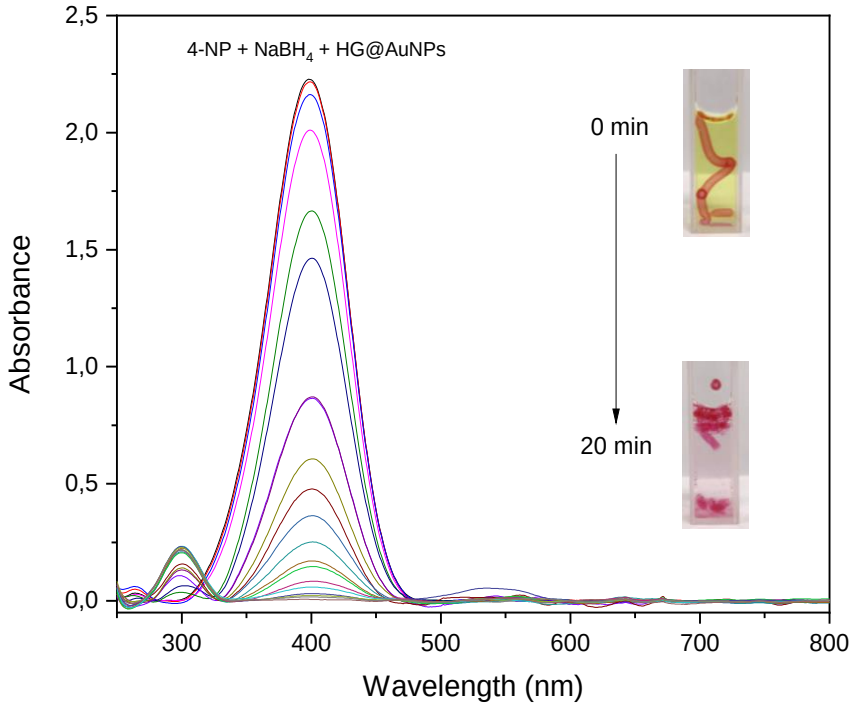

Figure 19. UV-vis spectra for reduction of 4-NP by $NaBH_4$ catalyzed by HG@AuNPs (69% of Au), at 25 °C.

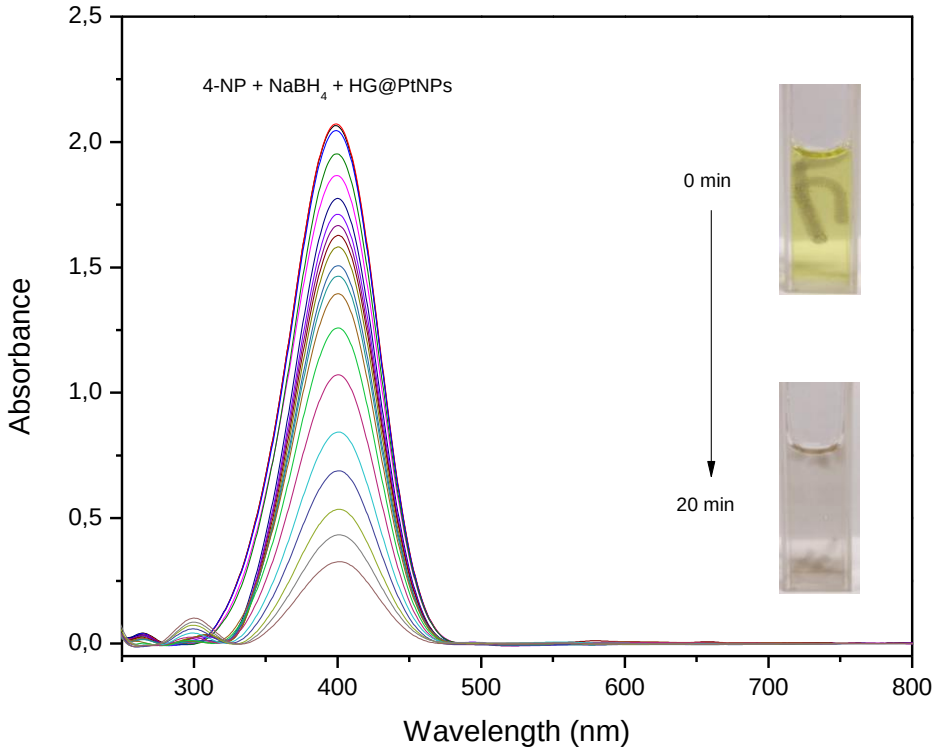

Figure 20. UV-vis spectra for reduction of 4-NP by $NaBH_4$ catalyzed by HG@PtNPs (107% of Pt), at 25 °C.

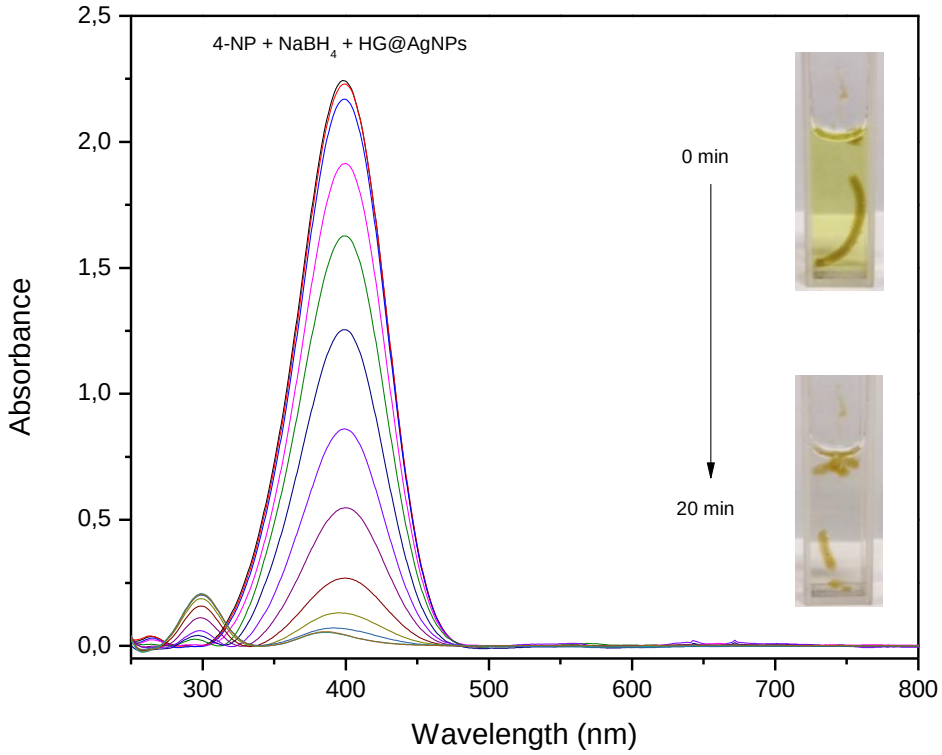

Figure 21. UV-vis spectra for reduction of 4-NP by $NaBH_4$ catalyzed by HG@AgNPs (52% of Ag), at 25 °C.

As seen in these absorption spectra, the kinetic reduction of 4-NP can be easily followed by UV-Vis spectroscopy due to changes in the spectrum: the absorption maximum for 4-NP at 317 nm (light yellow) is rapidly shifted to 400 nm when an excess of $NaBH_4$ is present due to the formation of 4-nitrophenolate ion (dark yellow). When the catalyst is added (*i.e.*, HG@M), after an induction time t_0 the reduction takes place, starting the decrease of band at 400 nm with a slowly increase in the peak at 300 nm as consequence of the formation of 4-aminophenol (4-AP). Originally, two isosbestic points must be present at ~280 and ~315 nm, but they can be shifted due to the presence of bubbles of H_2 gas that is generated in the reaction, affecting the optimal measurement.[55]

The kinetic reduction also was performed at 25 °C using hydrogels synthesized at 40 °C that showed a characteristic UV-Vis spectra with indicative of nanoparticles formation (*i. e.*, HG@Au40NPs and HG@Pt40NPs), with three different amounts (100, 200 and 300 mg of each hydrogel), and according to the UV-vis spectra obtained, the percentual conversion of 4-NP to 4-AP was calculated following the Equation 2. The results for all catalysts used are presented in Table 2 and was choose the best HG@M40 according to your yield of reduction

to calculate the linear correlation (k_{app}). The Figures 22 and 23 shows the reduction spectra specifically for those hydrogels that showed better catalytic activity.

Table 2. Conversion of 4-nitrophenolate ion with the formation of 4-AP (%), at variable amounts of metallic nanoparticles as catalyst (into hydrogels). Values were calculated based on the absorbance at 400 nm, with the reaction occurring for 20 min at 25 °C.

Catalyst	M^0 used in reduction (%)	Yield of reduction (%)
Au40	66	51
	46	17
	26	5
Pt40	98	75
	81	56
	40	21

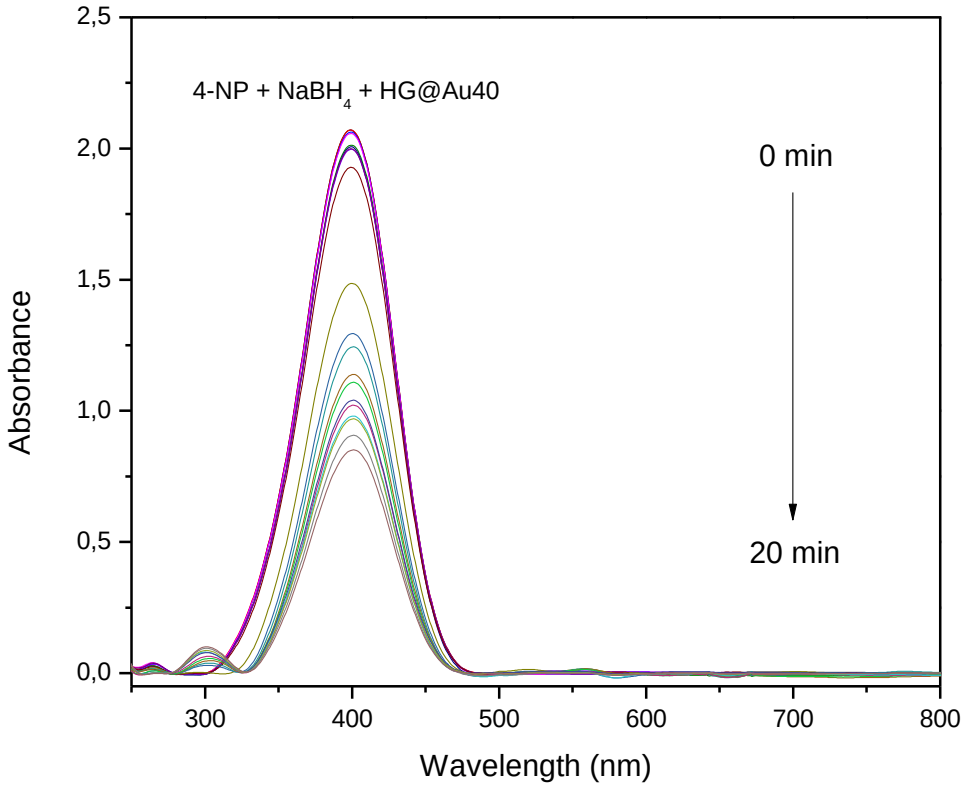

Figure 22. UV-vis spectra for reduction of 4-NP by $NaBH_4$ catalyzed by HG@Au40NPs (66% of Au), at 25 °C.

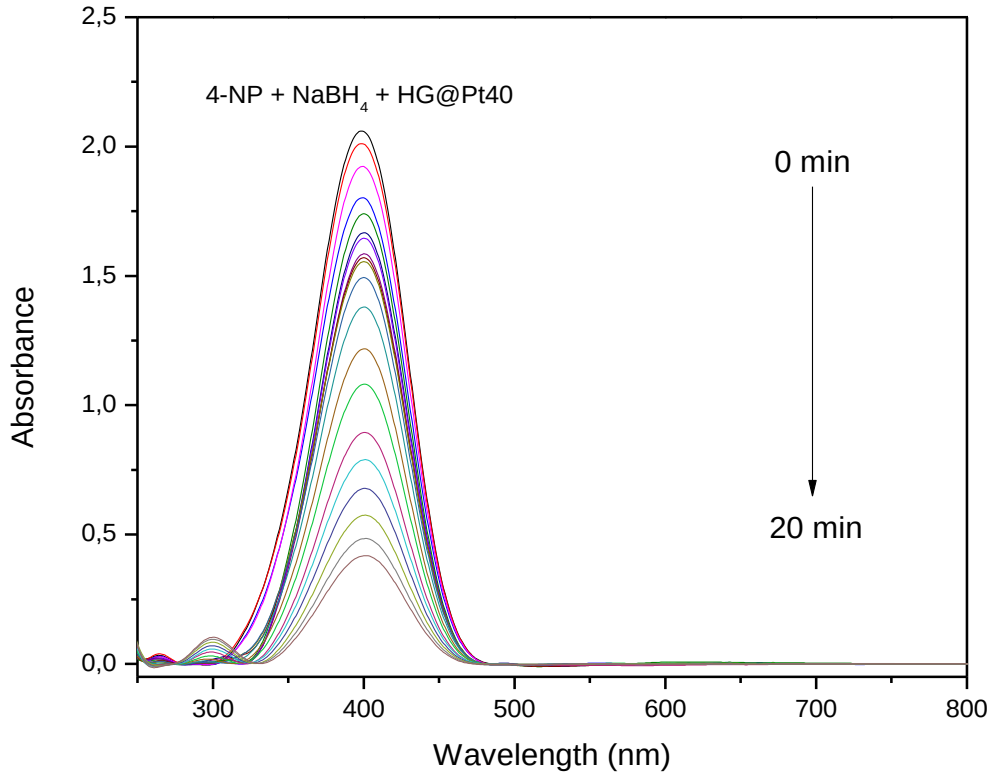

Figure 23. UV-vis spectra for reduction of 4-NP by $NaBH_4$ catalyzed by HG@Pt40NPs (98% of Pt), at 25 °C.

As expected, the hydrogels that were synthesized at 40 °C also presented a catalytic activity on reduction of 4-NP to 4-AP. However, comparing the hydrogels synthesized at 25 °C and 40 °C, the best percentage of reduction was higher in both the hydrogels made at 25 °C. When was used 69% of Au from HG@AuNPs, the conversion of nitrophenol to aminophenol was of 99%, but using an approximated amount of Au from HG@Au40NPs (66%) was possible obtain only 51% of reduction. These different results can be a consequence of different diameters of the nanoparticles, once that the size of nanoparticles is an important parameter in heterogeneous catalysis.

Since the work of Haber (1898),[56] various studies assume that the catalysis occurs on the surface of the metallic nanoparticle with an adsorption/desorption equilibrium of the 4-NP and BH_4^- in the surface,[57–59] that is, in terms of a Langmuir-Hinshelwood kinetics where both reactants must be firstly adsorbed on the surface to react.[55,60] According to Ayad *et al.* (2020), based on this model of kinetic, briefly, two catalytic mechanisms can be considered in the reduction of 4-NP: i) adsorption of BH_4^- on the surface of metallic nanoparticle with production of the hydrogen radical by electron transfer; and ii) adsorption of 4-NP with formation of 4-nitrophenolate ion that will be reacted with the adsorbed hydrogen species to form 4-AP by the

formation of 4-hydroxylaminophenol as intermediate.[61] Kong *et al.* (2017) also investigate these reduction process by mass spectrometry and detected intermediates that indicated that these commonly proposed mechanism is viable.[62] The Figure 24 presents an illustration of this process on the surface of metallic nanoparticle.

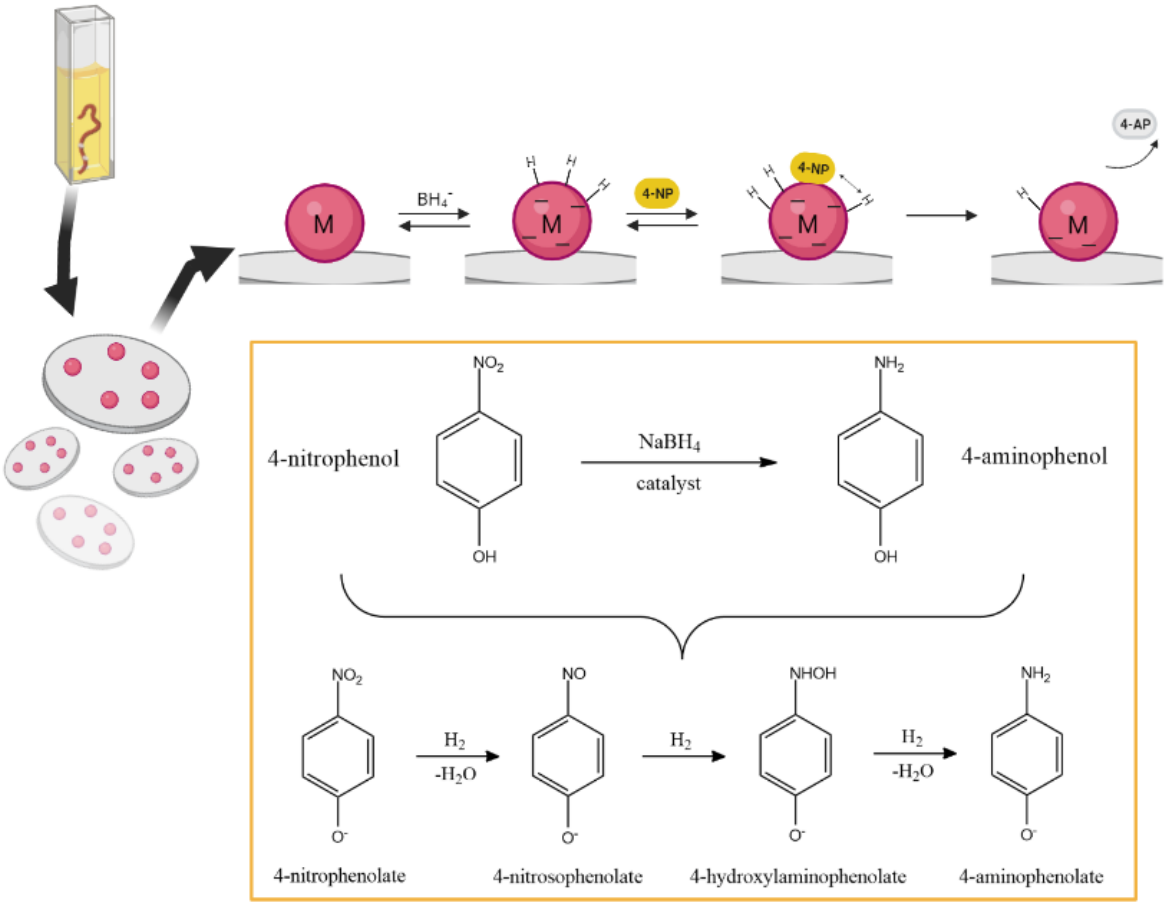

Figure 24. Illustration of proposed catalytic reduction of 4-nitrophenol (4-NP) by NaBH4 with a simplified mechanism of reaction. The reduction proceeds on the surface of the metal nanoparticles with an adsorption/desorption equilibrium of the reactants.

Since $NaBH_4$ was used in high excess in all catalytic reductions (about 100-fold higher than 4-NP, considering the initial concentrations), was expected that this reduction follows a pseudo first-order kinetics.[41,63–67] Based on this, the apparent reaction rate constant, k_{app}, for the best catalytic hydrogel of each type (HG@Au, Ag and Pt) was evaluated using the Equation 3:

$$\ln\left(\frac{A}{A_0}\right) = \ln\left(\frac{C}{C_0}\right) = -k_{app}\,.t \qquad \text{Eq. 3}$$

where A and A_0 are the absorbance at 400 nm relative to 4-nitrophenolate ion at every time and in the initial stage before addition of catalyst, respectively; and k_{app} is the apparent kinetic rate constant (at 25 °C). The plotted results are showed in Figure 25.

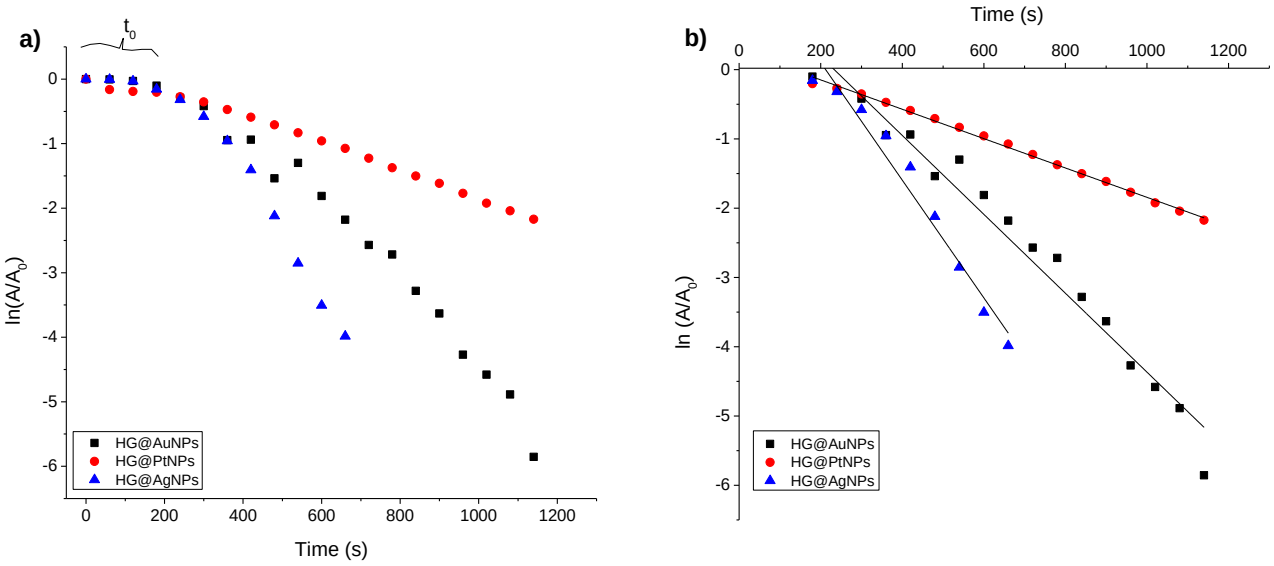

Figure 25. (a) Plots of ln(A/A0) vs time for the catalytic reduction of 4-NP by $NaBH_4$ in the presence of the hydrogels HG@M that presented best catalytic activity (at 25 ºC); and (b) the linear correlation plot to obtain the apparent rate constant (t_0 is not included).

In the Figure 25a is observed that in the initial stage (between 0 and 120 s to the three hydrogels) there is an induction time t_0 in which no significant reduction takes places.[59] Although the exact concept of t_0 is still unclear, some authors have suggested that the induction time is the period necessary for all dissolved oxygen to be consumed and not to compete with 4-NP and borohydride in interactions with surface of metallic nanoparticle [41,61,68]. However, others authors describe the induction time as the period in which occurs a surface reconstruction with the activation of the nanocatalysts surface and the adsorption of reactants[60,65,69]. After this time, the reaction starts following a pseudo first-order rate and from this linear part the k_{app} was taken according to the slope of linear fitting for each selected hydrogel (Figure 25b), and the values of k_{app} were presented in Table 3.

Table 3. Comparison of apparent rate constant (s^{-1}) of the three hydrogels for the reduction reaction, at 25 °C.

Catalyst	k_{app} (s^{-1})	R^2
HG@PtNPs	2.12 x 10^{-3}	0.996

HG@AuNPs	5.69 x 10^{-3}	0.969
HG@AgNPs	8.50 x 10^{-3}	0.962

In addition to the influence of the nanoparticle's characteristics in the kinetic rate of reduction, such as size of NPs[70], in this work was possible to note that the viscoelastic properties of hydrogels also can affect it, once the HG@Ag was the material with lowest value of storage modulus (G') (in the LRV), but the highest k_{app} value. This can be related to the rigidity of material and the diffusion of species into hydrogel matrix until reaching the surface of nanoparticles where occurs the reduction process. This relation is seen in all the three hydrogels, as demonstrated in Figure 26, once was obtained an increased k_{app} value according to decrease in their G' values.

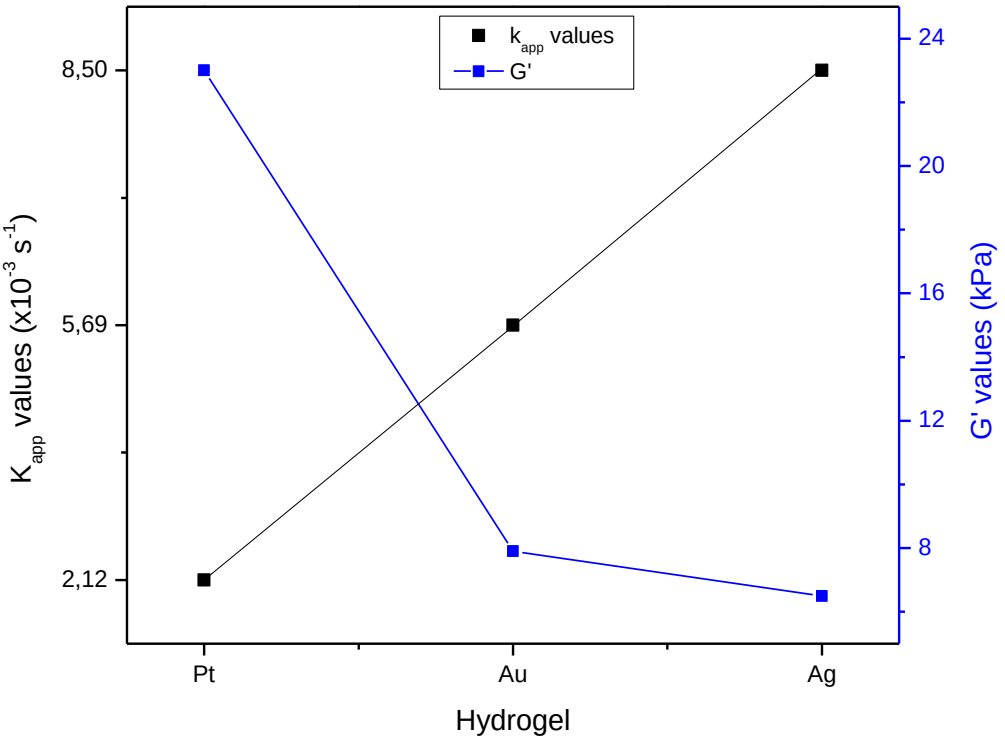

Figure 26. Relation between Storage modulus (G') and kapp values for hydrogels synthesized at 25 °C.

Similarly, to the hydrogels synthesized at 25 °C commented before, was calculated by Equation 3 the k_{app} values for hydrogels synthesized at 40 °C (Table 4).

Table 4. Comparison of apparent rate constant (s^{-1}) of the two hydrogels (40 °C) for the reduction reaction, at 25 °C.

Catalyst	k_{app} (s^{-1})	R^2
HG@Au40NPs	1.61 x 10^{-3}	0.988
HG@Pt40NPs	1.22 x 10^{-3}	0.956

As expected, the k_{app} for these hydrogels were lower than for their respective materials made at 25 °C, and this can be related with the nanoparticles size. Liu and co-works (2020) discussed that, under sufficient precursors, increasing temperature leads to an increase in the apparent constants k_1 and k_2 of nucleation and growth process (Figure 27), respectively, resulting in the formation of larger nanoparticles[46].

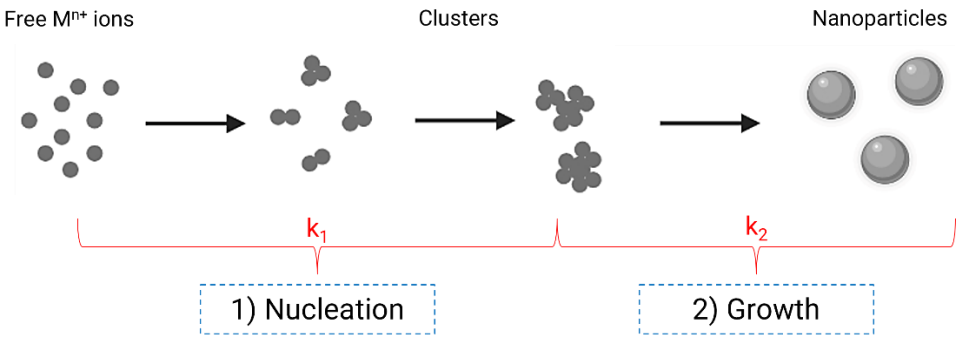

Figure 27. Representation of basic process for nanoparticles formation (nucleation and growth).

Furthermore, as mentioned before, based on UV-Vis spectra, is expected that these nanoparticles synthesized at 40 °C have a diameter slightly larger than the formed at 25 °C, and this will influence directly their catalytic activity [69].

3.2 Laponite-based nanohydrogels for delivery of anticancer drug cocktails

The nanohydrogels (NH) were formulated through inverse miniemulsion process as nanoemulsion in water-in-oil (w/o) biphasic system,[20] in which the Lap/SPA solution and the drugs' aqueous solution constitute the aqueous phase and the cyclohexane the oil phase (Figure 4). As nanoemulsion, the NHs appear transparent and are stable against sedimentation, which was confirmed by DLS measurements.[71] The mixture of phases was sonicated for 6 min to obtain inverse miniemulsion and this high-energy homogenization was chosen with the intention of producing nanodroplets with smaller size, once that this procedure generates

intensity pressure waves that propagate through liquids, forming microbubbles near the tip of the probe that oscillate violently.[72] As consequence of this oscillation, the microbubbles implode soon after, producing intense disruptive forces that efficiently breaks larger droplets into smaller.[72]

As seen in the Table 5, all nanohydrogels were synthesized with a size ratio lower than 200 nm, and this is important because the size of nanomaterial will directly impact their use as drug delivery system as mentioned in the introduction. The Figure 28 shows two nanohydrogels with single and co-encapsulation.

Table 5. Diameter (nm) obtained by DLS of synthesized hydrogels.

Nanohydrogel	Molar ratio	Diameter by DLS (nm)
NHCP	-	128 ± 39
NHFU	-	148 ± 38
NHCPA	-	152 ± 32
NHFUCP1	46:1	68 ± 12
NHFUCP2	11.5:1	70 ± 15
NHFUCP3	3:1	78 ± 13
NHCPCPA1	1:43	190 ± 30
NHCPCPA2	1:16	163 ± 34
NHCPCPA3	1.2:1	91 ± 16

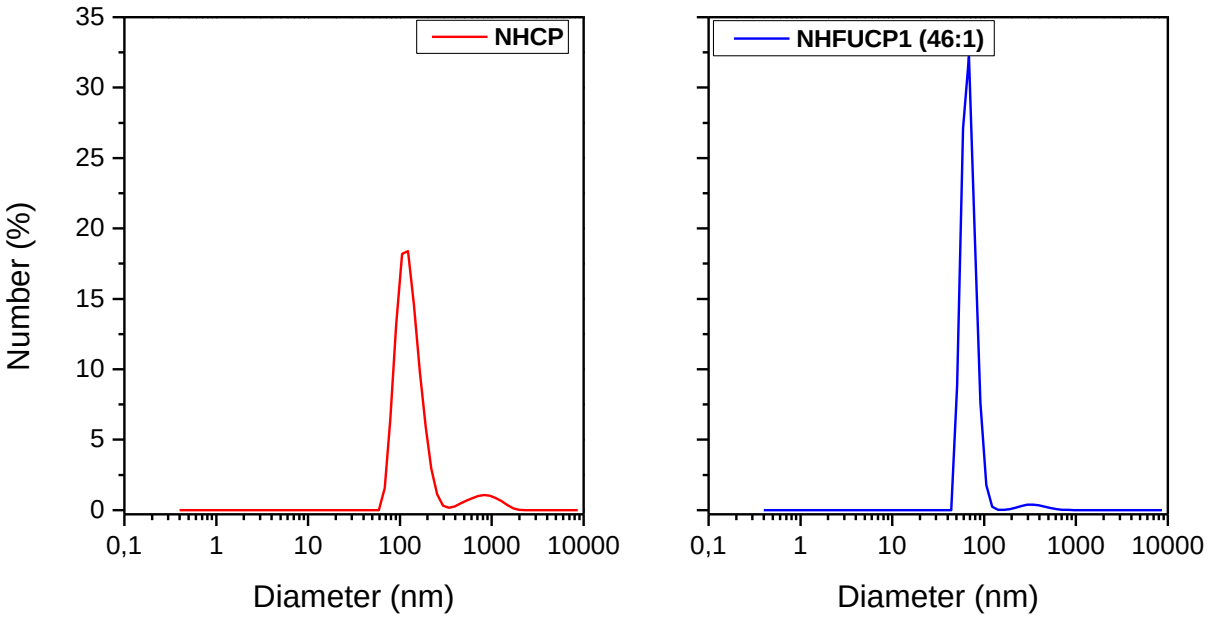

Figure 28. Hydrodynamic diameter (nm) of two diluted samples (10000x) obtained by DLS: NHCP, as example of nanohydrogel with only one drug encapsulated (red, at left), and NHFUCP1 as sample of NH with two drugs encapsulated (blue, at right).

All NH synthesized present zeta potential between -6 and -10 mV. The net negative value was expected since the SPA, polymer used with negative charge, will be preferentially wrapped in the positive edges of the nanodiscs, resulting as the outer layer of nanohydrogels the negatively charged surface of the Lap nanodiscs as mentioned before.

Since these hydrogel networks are formed by ionic interactions between Laponite nanodiscs and SPA, a neutral surfactant was used to stabilize the nanoemulsions and avoid possible interference that others charged surfactants could cause. Because of this, was used SPAN85, a nonionic and biodegradable surfactant with low HLB value which is ideal for w/o emulsion.[73] Furthermore, since the gelification of this material is based on ionic interactions, no radical initiator, UV, metallic catalysts or pH is used, which is an advantage since it will not damage the chemical structures of the guest molecules that will be encapsulated.

Lap nanodiscs slowly disintegrate at pH<7, liberating nontoxic species in the medium such as $Si(OH)_4$, Mg^{+2} and Na^{+}.[74] As commented before, the tumor microenvironment (TME) has a low pH and, because of these differences in pH (pH at 7.4 for the stable solutions of NHs in PBS medium against pH around 5 for the TME), is expected that the nanohydrogels act as pH-responsive nanomaterial protecting the encapsulated drugs in physiological conditions but releasing inside the tumor microenvironment at acidic medium. To simulate this condition, the

pH responsiveness of the nanohydrogel was investigated using DLS to measure the changes in its size when dispersed in acid solution. As seen in the Figure 29, when NHFUCP2 was dispersed in acetate buffer solution (pH 5.5), after 1h was observed a significant increase in size, which kept changing for the next hours. The increasing in the value of diameter over 24h suggests the absence of a well-formed nanomaterial, which could be associated with the swelling of the nanohydrogel over time until reaching 1648 nm, the point at which the material burst and disintegrates, as represented in the Figure 30.

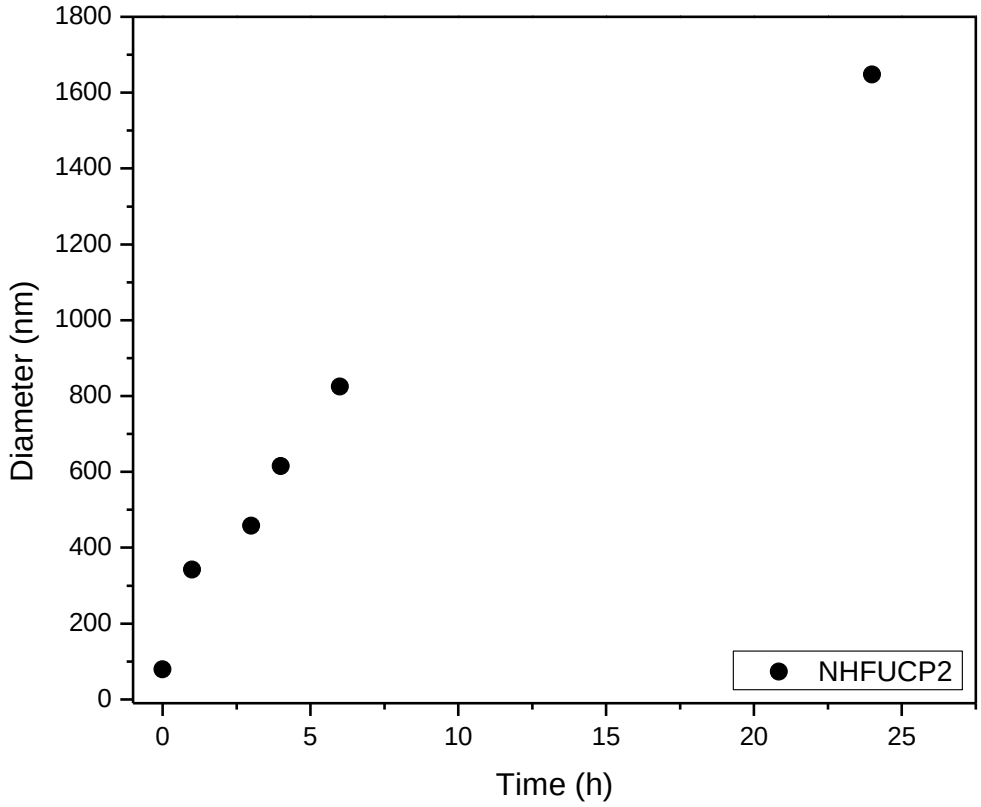

Figure 29. DLS data showing the changes in the size of NHFUCP, at pH 5.44 (37 °C), over time.

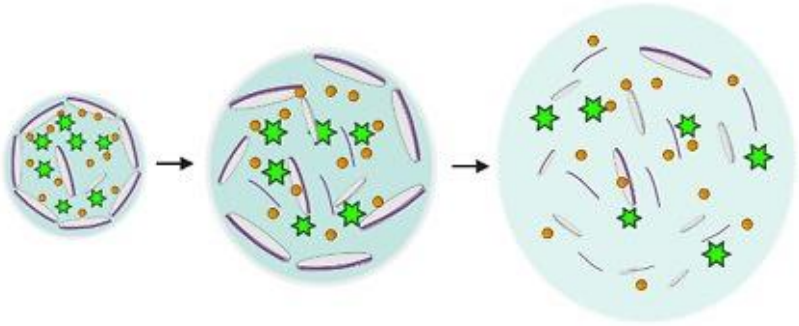

Figure 30. Representation of swell and burst processes of nanohydrogels in acidic medium.

Intending to evaluate the potential use of these NH as drug delivery system and, mainly, study the combination effect of different ratios between the encapsulated drugs against cancer cells, the nanomaterials were applied on MCF-7 and HeLa cells (breast and cervical cancers, respectively). The IC_{50} values (*i.e.*, the dose of a drug that causes an inhibition of 50% in a population after a time)[76] for the nanohydrogels tested in the cancer cells are presented in Table 6, and the preliminary tests of cell viability were made using CCK-8 kit, which is a colorimetric method based on the bioreduction of WST-8 (monosodium 2-(2-methoxy-4-nitrophenyl)-3-(4-nitrophenyl)-5-(2,4-disulfophenyl)-2H-tetrazolium salt) by cellular dehydrogenases with formation of orange product. The amount of these orange product is directly proportional to the number of living cells and because of this is possible determinate the cell viability by colorimetric assay.

Table 6. IC50 values obtained by nanohydrogels with different ratios between the drugs after 48h of incubation.

Nanohydrogel	**Molar ratio[1]**	**IC_{50} (μM)**	
		MCF-7	**HeLa**
NHCP	-	23.9 ± 0.04	22 ± 0.01
NHFU	-	1134	*
NHCPA	-	*	*
NHFUCP1	46:1	289.7 ± 0.08 (total drug)	1927 ± 0.05 (total drug)
NHFUCP2	11.5:1	140.9 ± 0.10 (total drug)	135.1 ± 0.03 (total drug)
NHFUCP3	3:1	556.1 ± 0.09 (total drug)	149.8 ± 0.12 (total drug)
NHCPCPA1	1:43	72.64 ± 0.14 (total drug)	*
NHCPCPA2	1:16	40.47 ± 0.18 (total drug)	228.3 ± 0.06 (total drug)
NHCPCPA3	1.2:1	67.03 ± 0.11 (total drug)	*

[1]The molar ratio are presented as concentration of 5-FU to CP in NHFUCP nanohydrogels, and CP to CPA in NHCPCPA materials. *It was not possible obtain a IC_{50} because did not reach 50% of cell viability. The IC_{50} values for aqueous solution of CP applied alone in MCF-7 and HeLa were, respectively, 30.15 and 27.3 μM. The IC_{50} value for aqueous solution of 5-FU applied alone in MCF-7 cells was 1356 μM, and for HeLa cells did not reach 50% of cell viability. The IC_{50} value for aqueous solution of CPA did not reach 50% of viability in both MCF-7 and HeLa cells.

Taking into consideration the materials that reached 50% of cell viability (*i. e.*, that has an IC_{50} value) with single drugs and the relative proportions in NHs combinations, the sum of the drug effects would result in the following IC_{50} values for MCF-7 cells: 1110.5 μM for

NHFUCP1, 1045.4 μM for NHFUCP2, and 848.1 μM for NHFUCP3. For all three nanohydrogels the real values obtained (as seen in the Table 6) were lower than the values expected for the amount of the drugs effect, with a better result being obtained with the NHFUCP2 which is composed of approximately 92% of 5-FU and 8% of CP (140.9 μM for MCF-7 cells, at 48h). These data suggest that NHs presents an overall positive effect on the drug cocktail delivery for MCF-7 cells, since the actual inhibition effect obtained was greater than the expected when calculated based on the relative proportions of drugs in the combinations. Moreover, the nanohydrogels that combine Cisplatin and Cyclophosphamide (NHCPCPA) presented IC_{50} values very low when applied in MCF-7 cells, with the best material resulting in an IC_{50} of 40.47 μM, which means an increase in the cytotoxic effect of when combined these two drugs, differently of the NH with only CPA (NHCPA) that did not even reach 50% of viability in MCF-7 cells.

One way to analyze the relation between the drugs mixed in the nanohydrogels is calculating the CI index for each NHFUCP according to the classic equation of Chou-Talalay [35] (Eq. 1), where CI<0.9 indicate synergistic effect between drugs; CI = 0.9 to 1.1 corresponds to an additive interaction (enhancement of one drug to other); and CI>1.1 an antagonistic effect. For MCF-7 cells, considering the values for free drugs in aqueous solutions and the dose of each drug in the NHFUCP that inhibited 50% of cells (*i.e.,* the IC_{50} value achieved for each drug in the combination), two combinations resulted in synergistic effect, NHFUCP1 and NHFUCP2, with CI of 0.88 and 0.5, respectively. For NHFUCP3, however, was obtained a CI value higher than 1 which indicates that this combination had an antagonistic effect between 5-FU and CP. Interestingly, the nanohydrogels combinations with a higher amount of 5-Fluorouracil over Cisplatin were those that presented better results and synergistic effect (both nanohydrogels with 5-FU more than 90% of total drug dosage). It was known that the combinatory effect between drugs were associated with the drugs ratios[77] and the synergism was observed just at certain ratios of drugs in combination.[35] Fu *et al.* (2020) applied a lipid-polymer hybrid nanoparticle with co-encapsulated CP and 5-FU (at different ratios) in BE-3 cells (human esophageal cancer cell line), for 24h, and obtained a synergistic effect with combinations that had intermediate proportions, with lower CI value resulted from a combination with an 2-fold excess (w/w) of 5-FU over CP.[78]

When applied in HeLa cells, however, the maximum concentration of NHFU and NHCPA results in a cell viability of only 64% and 73%, respectively, and this can be related to the lower sensitivity of HeLa cells to 5-FU and CPA than MCF-7 cells. Blanco *et al.* (2011)

also obtained a lower cytotoxicity of 5-FU-loaded folate-conjugated submicrogels when applied in HeLa cells, reaching approximately 60% of viability at 48h, while for MCF-7 cells in the same conditions of concentration and time, was reached approximately 20% of viability [79].

The CI values were calculated only for NHFUCP combinations applied in MCF-7 cells because was not possible obtain values for applications these materials in HeLa cells since in these cell lines was not reached a viability of 50% for free 5-FU aqueous solution and, according to Eq.1, to calculate the CI values is necessary the dose (IC_{50} in this case) at both single free and mixed drug (5-FU and NHFUCP, respectively) in the material. Also, was not possible to calculate the CI values for NHCPCPA in both MCF-7 and HeLa cells for the same reason explained above (neither CPA aqueous solution nor NHCPA reached a viability of 50%).

4. CONCLUSION

The results obtained in this work, indicate the development of Au, Ag and Pt nanoparticles via *in situ* synthesis into Laponite/SPA hydrogels, where the formation and stability of these NPs was followed by UV-Vis spectroscopy. The TEM images confirmed the formation of spherical Pt and Ag NPs, with sizes between 1-2 nm and 2-3 nm, respectively, which is an interesting size to be applied as a nanocatalyst, since smaller metallic nanoparticles have a higher surface area. To investigate the application of these materials as heterogeneous catalysts was used a reaction model based on the reduction of 4-nitrophenol to 4-aminophenol with $NaBH_4$ as a reducing agent. For this reduction, the materials acted very well as catalysts and was analyzed the influence of the hydrogel's amount in the reduction kinetic, getting a conversion between 80-99% for the best materials between the hydrogels with Au, Ag, and Pt. Also, in addition to the influence of nanoparticles size over the kinetic reduction rate, was noted that the rheological properties of hydrogels also influence the apparent constant of reduction, decreasing the catalytic activity with the increase in the rigidity of hydrogels (*i. e.*, $\downarrow k_{app}$ with ↑storage modulus – G'). Finally, was evaluated the effect of a higher temperature on the synthesis of the hydrogels (synthesis at 40 °C), but despite they have been formed in a shorter time than the materials synthesized at 25 °C, there was a decrease in the catalytic activity of the best materials.

As drug delivery systems in the nanoscale, the Laponite-based nanohydrogels were synthesized within the size range adequate for drug delivery applications (60-190 nm). Nanohydrogels with combinations of two anticancer drugs co-encapsulated (combinations between Cisplatin, CP + 5-Fluorouracil, 5-FU; and Cisplatin, CP + Cyclophosphamide, CPA) were synthesized with varied ratios and applied against MCF-7 and HeLa cells to verify the effect of different molar ratios between anticancer drugs. When applied in MCF-7 cancer cells, two of the three proportions (NHFUCP1 and NHFUCP2, with molar ratio of, respectively, 46:1 and 11.5:1 for 5-FU:CP) resulted in a synergistic effect with CI<0.9, while the third combination resulted in antagonistic effect (NHFUCP3, 3:1 for 5-FU:CP). For combinations between CP+CPA (NHCPCPA), all nanohydrogels when applied in MCF-7 cells resulted in a lower IC_{50} value than the nanohydrogel with single drug, which means an increase in the cytotoxic effect when mixed those two drugs. The results were interesting since indicates the influence of the ratios between the drugs co-encapsulated against the cell viability.

The results obtained showed the incredible versatility of Laponite-based materials for applications from catalysis as support material to metallic nanocatalysts, to drug delivery as nanohydrogels acting as nanocarriers.

5. REFERENCES

1. Chai, Q., Jiao, Y. & Yu, X. Hydrogels for biomedical applications: Their characteristics and the mechanisms behind them. *Gels* **3**, (2017).

2. Zhao, L. Z. *et al.* Recent advances in clay mineral-containing nanocomposite hydrogels. *Soft Matter* **11**, 9229–9246 (2015).

3. Takeno, H. & Nakamura, W. Structural and mechanical properties of composite hydrogels composed of clay and a polyelectrolyte prepared by mixing. *Colloid Polym. Sci.* **291**, 1393–1399 (2013).

4. Becher, T. B. *et al.* The structure-property relationship in LAPONITE® materials: From Wigner glasses to strong self-healing hydrogels formed by non-covalent interactions. *Soft Matter* **15**, 1278–1289 (2019).

5. Nicolai, T. & Cocard, S. Dynamic light-scattering study of aggregating and gelling colloidal disks. *J. Colloid Interface Sci.* **244**, 51–57 (2001).

6. Tawari, S. L., Koch, D. L. & Cohen, C. Electrical double-layer effects on the Brownian diffusivity and aggregation rate of Laponite clay particles. *J. Colloid Interface Sci.* **240**, 54–66 (2001).

7. Ruzicka, B. *et al.* Observation of empty liquids and equilibrium gels in a colloidal clay. *Nat. Mater.* **10**, 56–60 (2011).

8. Becher, T. B. & Ornelas, C. Nonswellable Injectable Hydrogels Self-Assembled Through Non-Covalent Interactions. *ChemistrySelect* **2**, 3009–3013 (2017).

9. Sahiner, N. In situ metal particle preparation in cross-linked poly (2-acrylamido-2-methyl-1-propansulfonic acid) hydrogel networks. *Colloid Polym. Sci.* **285**, 283–292 (2006).

10. Sahiner, N. Colloidal nanocomposite hydrogel particles. *Colloid Polym. Sci.* **285**, 413–421 (2007).

11. Ai, L. & Jiang, J. Catalytic reduction of 4-nitrophenol by silver nanoparticles stabilized on environmentally benign macroscopic biopolymer hydrogel. *Bioresour. Technol.* **132**, 374–377 (2013).

12. Seo, Y. S. *et al.* Catalytic reduction of 4-nitrophenol with gold nanoparticles

synthesized by caffeic acid. *Nanoscale Res. Lett.* **12**, (2017).

13. Haraguchi, K. & Varade, D. Platinum-polymer-clay nanocomposite hydrogels via exfoliated clay-mediated in situ reduction. *Polymer (Guildf).* **55**, 2496–2500 (2014).

14. Sápi, A. *et al.* Metallic Nanoparticles in Heterogeneous Catalysis. *Catal. Letters* **151**, 2153–2175 (2021).

15. Chen, G., Roy, I., Yang, C. & Prasad, P. N. Nanochemistry and Nanomedicine for Nanoparticle-based Diagnostics and Therapy. *Chem. Rev.* **116**, 2826–2885 (2016).

16. Dalwadi, C. & Patel, G. Application of Nanohydrogels in Drug Delivery Systems: Recent Patents Review. *Recent Pat. Nanotechnol.* **9**, 17–25 (2015).

17. Gonçalves, C., Pereira, P. & Gama, M. Self-assembled hydrogel nanoparticles for drug delivery applications. *Materials (Basel).* **3**, 1420–1460 (2010).

18. Fuciños, C. *et al.* Use of Poly(N-isopropylacrylamide) Nanohydrogels for the Controlled Release of Pimaricin in Active Packaging. *J. Food Sci.* **77**, (2012).

19. D'Arrigo, G. *et al.* Self-assembled gellan-based nanohydrogels as a tool for prednisolone delivery. *Soft Matter* **8**, 11557–11564 (2012).

20. Becher, T. B. *et al.* Soft Nanohydrogels Based on Laponite Nanodiscs: A Versatile Drug Delivery Platform for Theranostics and Drug Cocktails. *ACS Appl. Mater. Interfaces* **10**, 21891–21900 (2018).

21. Iranpour, S., Bahrami, A. R., Sh. Saljooghi, A. & Matin, M. M. Application of smart nanoparticles as a potential platform for effective colorectal cancer therapy. *Coord. Chem. Rev.* **442**, 213949 (2021).

22. Yu, L. *et al.* Reduction-sensitive N, N'-Bis(acryloyl) cystinamide-polymerized Nanohydrogel as a Potential Nanocarrier for Paclitaxel Delivery. *Des. Monomers Polym.* **24**, 98–105 (2021).

23. Zha, L., Banik, B. & Alexis, F. Stimulus responsive nanogels for drug delivery. *Soft Matter* **7**, 5908–5916 (2011).

24. Bhattacharya, S. Fabrication of poly(sarcosine), poly (ethylene glycol), and poly (lactic-co-glycolic acid) polymeric nanoparticles for cancer drug delivery. *J. Drug Deliv. Sci. Technol.* **61**, (2021).

25. McDonald, D. M. & Baluk, P. Significance of blood vessel leakiness in cancer. *Cancer Res.* **62**, 5381–5385 (2002).

26. Taghizadeh, B. *et al.* Classification of stimuli-responsive polymers as anticancer drug delivery systems. *Drug Deliv.* **22**, 145–155 (2015).

27. Hashizume, H. *et al.* Openings between defective endothelial cells explain tumor vessel leakiness. *Am. J. Pathol.* **156**, 1363–1380 (2000).

28. Subhan, M. A., Yalamarty, S. S. K., Filipczak, N., Parveen, F. & Torchilin, V. P. Recent advances in tumor targeting via epr effect for cancer treatment. *J. Pers. Med.* **11**, (2021).

29. Yoo, J., Park, C., Yi, G., Lee, D. & Koo, H. Active targeting strategies using biological ligands for nanoparticle drug delivery systems. *Cancers (Basel).* **11**, (2019).

30. Asgari, M., Soleymani, M., Miri, T. & Barati, A. Design of thermosensitive polymer-coated magnetic mesoporous silica nanocomposites with a core-shell-shell structure as a magnetic/temperature dual-responsive drug delivery vehicle. *Polym. Adv. Technol.* 1–9 (2021). doi:10.1002/pat.5417

31. Li, J. *et al.* Rapid pH-responsive self-disintegrating nanoassemblies balance tumor accumulation and penetration for enhanced anti-breast cancer therapy. *Acta Biomater.* (2021). doi:10.1016/j.actbio.2021.04.022

32. Boedtkjer, E. & Pedersen, S. F. The Acidic Tumor Microenvironment as a Driver of Cancer. *Annu. Rev. Physiol.* **82**, 103–126 (2020).

33. Yin, Z., Deng, Z., Zhao, W. & Cao, Z. Searching synergistic dose combinations for anticancer drugs. *Front. Pharmacol.* **9**, 1–7 (2018).

34. Celebi, R., Bear Don't Walk, O., Movva, R., Alpsoy, S. & Dumontier, M. In-silico Prediction of Synergistic Anti-Cancer Drug Combinations Using Multi-omics Data. *Sci. Rep.* **9**, 1–10 (2019).

35. Chou, T. C. Drug combination studies and their synergy quantification using the chou-talalay method. *Cancer Res.* **70**, 440–446 (2010).

36. Basu, A. & Krishnamurthy, S. Cellular responses to cisplatin-induced DNA damage. *J. Nucleic Acids* **2010**, (2010).

37. Ghosh, S. Cisplatin: The first metal based anticancer drug. *Bioorg. Chem.* **88**, 102925 (2019).

38. Dimery, I. W., Legha, S. S., Shirinian, M. & Waun Ki Hong. Fluorouracil, doxorubicin, cyclophosphamide, and cisplatin combination chemotherapy in advanced or recurrent salivary gland carcinoma. *J. Clin. Oncol.* **8**, 1056–1062 (1990).

39. Longley, D. B., Harkin, D. P. & Johnston, P. G. 5-Fluorouracil: Mechanisms of action and clinical strategies. *Nat. Rev. Cancer* **3**, 330–338 (2003).

40. Hasanah, Y. I. F., Harahap, Y. & Purwanto, D. J. Phenotyping study of cyclophosphamide 4-hydroxylation in malay cancer patients. *Drug Des. Devel. Ther.* **15**, 305–313 (2021).

41. Menumerov, E., Hughes, R. A. & Neretina, S. Catalytic Reduction of 4-Nitrophenol: A Quantitative Assessment of the Role of Dissolved Oxygen in Determining the Induction Time. *Nano Lett.* **16**, 7791–7797 (2016).

42. Dolya, N. *et al.* 'One-pot' in situ formation of gold nanoparticles within poly(acrylamide) hydrogels. *Macromol. Chem. Phys.* **214**, 1114–1121 (2013).

43. Martínez-Higuera, A. *et al.* Hydrogel with silver nanoparticles synthesized by Mimosa tenuiflora for second-degree burns treatment. *Sci. Rep.* **11**, 1–16 (2021).

44. Salem, M. A., Bakr, E. A. & El-Attar, H. G. Pt@Ag and Pd@Ag core/shell nanoparticles for catalytic degradation of Congo red in aqueous solution. *Spectrochim. Acta - Part A Mol. Biomol. Spectrosc.* **188**, 155–163 (2018).

45. Varade, D. & Haraguchi, K. Synthesis of highly active and thermally stable nanostructured Pt/Clay materials by clay-mediated in situ reduction. *Langmuir* **29**, 1977–1984 (2013).

46. Liu, H., Zhang, H., Wang, J. & Wei, J. Effect of temperature on the size of biosynthesized silver nanoparticle: Deep insight into microscopic kinetics analysis. *Arab. J. Chem.* **13**, 1011–1019 (2020).

47. Begum, R. *et al.* Applications of UV/Vis Spectroscopy in Characterization and Catalytic Activity of Noble Metal Nanoparticles Fabricated in Responsive Polymer Microgels: A Review. *Crit. Rev. Anal. Chem.* **48**, 503–516 (2018).

48. Pálková, H., Madejová, J., Zimowska, M. & Serwicka, E. M. Laponite-derived porous clay heterostructures: II. FTIR study of the structure evolution. *Microporous Mesoporous Mater.* **127**, 237–244 (2010).

49. Skelton, S. *et al.* Biomimetic adhesive containing nanocomposite hydrogel with enhanced materials properties. *Soft Matter* **9**, 3825–3833 (2013).

50. Cuomo, F., Cofelice, M. & Lopez, F. Rheological characterization of hydrogels from alginate-based nanodispersion. *Polymers (Basel).* **11**, (2019).

51. Du, X., Zhou, J., Shi, J. & Xu, B. Supramolecular Hydrogelators and Hydrogels: From Soft Matter to Molecular Biomaterials. *Chem. Rev.* **115**, 13165–13307 (2015).

52. Li, M. & Chen, G. Revisiting catalytic model reaction p-nitrophenol/NaBH4 using metallic nanoparticles coated on polymeric spheres. *Nanoscale* **5**, 11919–11927 (2013).

53. Zhao, B. *et al.* Degradation of 4-nitrophenol (4-NP) using Fe-TiO2 as a heterogeneous photo-Fenton catalyst. *J. Hazard. Mater.* **176**, 569–574 (2010).

54. Sahiner, N., Ozay, H., Ozay, O. & Aktas, N. New catalytic route: Hydrogels as templates and reactors for in situ Ni nanoparticle synthesis and usage in the reduction of 2- and 4-nitrophenols. *Appl. Catal. A Gen.* **385**, 201–207 (2010).

55. Gu, S. *et al.* Kinetic analysis of the catalytic reduction of 4-nitrophenol by metallic nanoparticles. *J. Phys. Chem. C* **118**, 18618–18625 (2014).

56. Haber, F. Z. Gradual Electrolytic Reduction of Nitrobenzene with Limited Cathode Potential. *Elektrochem. Angew. Phys. Chem.* **22**, 506−514 (1898).

57. Nigra, M. M., Ha, J. M. & Katz, A. Identification of site requirements for reduction of 4-nitrophenol using gold nanoparticle catalysts. *Catal. Sci. Technol.* **3**, 2976–2983 (2013).

58. Layek, K. *et al.* Gold nanoparticles stabilized on nanocrystalline magnesium oxide as an active catalyst for reduction of nitroarenes in aqueous medium at room temperature. *Green Chem.* **14**, 3164–3174 (2012).

59. Wunder, S., Polzer, F., Lu, Y., Mei, Y. & Ballauff, M. Kinetic analysis of catalytic reduction of 4-nitrophenol by metallic nanoparticles immobilized in spherical polyelectrolyte brushes. *J. Phys. Chem. C* **114**, 8814–8820 (2010).

60. Wunder, S., Lu, Y., Albrecht, M. & Ballauff, M. Catalytic activity of faceted gold nanoparticles studied by a model reaction: Evidence for substrate-induced surface restructuring. *ACS Catal.* **1**, 908–916 (2011).

61. Ayad, A. I., Luart, D., Dris, A. O. & Guénin, E. Kinetic analysis of 4-nitrophenol reduction by "water-soluble" palladium nanoparticles. *Nanomaterials* **10**, 1–16 (2020).

62. Kong, X., Zhu, H., Chen, C. Le, Huang, G. & Chen, Q. Insights into the reduction of 4-nitrophenol to 4-aminophenol on catalysts. *Chem. Phys. Lett.* **684**, 148–152 (2017).

63. Velpula, S., Beedu, S. R. & Rupula, K. Bimetallic nanocomposite (Ag-Au, Ag-Pd, Au-Pd) synthesis using gum kondagogu a natural biopolymer and their catalytic potentials in the degradation of 4-nitrophenol. *Int. J. Biol. Macromol.* **190**, 159–169 (2021).

64. Kästner, C. & Thünemann, A. F. Catalytic Reduction of 4-Nitrophenol Using Silver Nanoparticles with Adjustable Activity. *Langmuir* **32**, 7383–7391 (2016).

65. Singh, J. *et al.* Enhanced catalytic reduction of 4-nitrophenol and congo red dye By silver nanoparticles prepared from Azadirachta indica leaf extract under direct sunlight exposure. *Part. Sci. Technol.* **37**, 430–439 (2019).

66. Geng, Q. & Du, J. Reduction of 4-nitrophenol catalyzed by silver nanoparticles supported on polymer micelles and vesicles. *RSC Adv.* **4**, 16425–16428 (2014).

67. Pandey, S. & Mishra, S. B. Catalytic reduction of p-nitrophenol by using platinum nanoparticles stabilised by guar gum. *Carbohydr. Polym.* **113**, 525–531 (2014).

68. Lu, Y., Mei, Y., Ballauff, M. & Drechsler, M. Thermosensitive core-shell particles as carrier systems for metallic nanoparticles. *J. Phys. Chem. B* **110**, 3930–3937 (2006).

69. Zhou, X., Xu, W., Liu, G., Panda, D. & Chen, P. Size-dependent catalytic activity and dynamics of gold nanoparticles at the single-molecule level. *J. Am. Chem. Soc.* **132**, 138–146 (2010).

70. Jia, L. *et al.* Facile fabrication of highly active magnetic aminoclay supported palladium nanoparticles for the room temperature catalytic reduction of nitrophenol and nitroanilines. *Nanomaterials* **8**, (2018).

71. Forgiarini, A., Esquena, J., González, C. & Solans, C. Formation of nano-emulsions by low-energy emulsification methods at constant temperature. *Langmuir* **17**, 2076–2083

(2001).

72. Leong, T. S. H., Martin, G. J. O. & Ashokkumar, M. Ultrasonic encapsulation – A review. *Ultrason. Sonochem.* **35**, 605–614 (2017).

73. Sondari, D. & Tursiloadi, S. The effect of surfactan on formulation and stability of nanoemulsion using extract of Centella Asiatica and Zingiber Officinale. *AIP Conf. Proc.* **2049**, (2018).

74. Becher, T. B. *et al.* The structure-property relationship in LAPONITE® materials: From Wigner glasses to strong self-healing hydrogels formed by non-covalent interactions. *Soft Matter* **15**, 1278–1289 (2019).

75. Garg, T., Singh, S. & Goyal, A. K. Stimuli-sensitive hydrogels: An excellent carrier for drug and cell delivery. *Crit. Rev. Ther. Drug Carrier Syst.* **30**, 369–409 (2013).

76. González-Larraza, P. G. *et al.* IC50Evaluation of Platinum Nanocatalysts for Cancer Treatment in Fibroblast, HeLa, and DU-145 Cell Lines. *ACS Omega* **5**, 25381–25389 (2020).

77. Chou, T. C. Theoretical basis, experimental design, and computerized simulation of synergism and antagonism in drug combination studies. *Pharmacol. Rev.* **58**, 621–681 (2006).

78. Fu, Q., Wang, J. & Liu, H. Chemo-immune synergetic therapy of esophageal carcinoma: trastuzumab modified, cisplatin and fluorouracil co-delivered lipid–polymer hybrid nanoparticles. *Drug Deliv.* **27**, 1535–1543 (2020).

79. Blanco, M. D. *et al.* In vitro and in vivo evaluation of a folate-targeted copolymeric submicrohydrogel based on N-isopropylacrylamide as 5-fluorouracil delivery system. *Polymers (Basel).* **3**, 1107–1125 (2011).